Controlled Leaky-Wave Radiation From a Planar Configuration of Width-Modulated Microstrip Lines

Symon K. Podilchak, *Member, IEEE*, Ladislau Matekovits, *Senior Member, IEEE*, Alois P. Freundorfer, *Senior Member, IEEE*, Yahia M. M. Antar, *Fellow, IEEE*, and Mario Orefice, *Senior Member, IEEE*

***Abstract*—Planar leaky-wave antenna (LWA) designs that utilize a printed surface wave (SW) source are presented. Specifically, by the addition of a periodic arrangement of width-modulated microstrip lines on top of a grounded dielectric slab (GDS), a sinusoidally modulated reactance surface (SMRS) can be realized, providing appropriate conditions for leaky wave (LW) radiation. In addition, a transition section near the SW source improves antenna matching, while also, controlling the leakage rate and aperture distribution. A numerically computed dispersion diagram (DD) for the periodic structure is also calculated in terms of Mathieu functions. Full-wave simulations and measurements are in agreement with the developed numerical model and results suggest that these LWAs can offer broadside radiation as well as continuous beam scanning with radiation efficiencies of more than 85%. In addition, the investigated width-modulated microstrip lines offer ease of fabrication and may also be useful in the design of new periodic structures for wave guidance and other low-cost printed circuits and antennas.**

***Index Terms*—Leaky-wave antenna (LWA), leaky waves (LWs), microstrip, periodic structure, surface waves (SWs).**

I. Introduction

HOLOGRAPHIC antennas have received much interest in the electromagnetics community [1]–[6]. These antenna designs are characterized by a suitable aperture and source configuration. Similarly, by utilizing surface-waves (SWs) and periodic metallic strips, leaky-waves (LWs) can be excited [7]–[9], realizing the transformation from a bound and guided-wave mode to a radiated mode. The beam patterns generated by this type of planar leaky-wave antenna (LWA) [10]–[12] can be thought of as having similarities to optical hologram formation at microwave and millimeter wave frequencies. Applications include radar, surveillance systems, and satellite communications. In general, these planar topologies are well accepted due to their ease of fabrication and integration with other printed devices.

Recent examples of such LWA structures [13]–[16] can include an engineered guiding surface that achieves a periodic variation of the effective material parameters [17]–[19] defining a sinusoidally modulated reactance surface (SMRS). This classic modulation technique can achieve LW radiation, as in [13]–[16], but can also be exploited for non-radiating applications. For example, in [20] a 2-D periodic structure was investigated with sinusoidal variation of the material parameters, but after the separation of variables, results were reduced to a pair of coupled differential equations. Solutions were presented but limited explanations were given on how such a structure can be attained in practice. In [21] an infinite periodic structure was realized by employing a closed toroidal artificial transmission line where the phase velocity was periodically modulated (by varying the reactive loading) to demonstrate controlled propagation, while in [22], a periodic structure was proposed using a multi-layer microstrip guide. In particular, the unit cell in [22] consisted of a width modulated line, immersed in a multilayer stackup of substrate materials with a single bottom ground plane. In that work the width of the microstrip line was varied in such a way, to guarantee a sinusoidal behavior of the effective dielectric constant. These concepts for non-radiating applications were then extended in [13] and [16] to SW driven planar LWAs where power leakage was achieved from such an array of width-modulated microstrip lines printed on a single-layer, grounded dielectric slab (GDS). Other guided-wave applications using such planar structures include transmission-line based sensors and real-time monitoring systems as discussed in [23].

A new class of planar LWA that makes use of the structures previously discussed in [16] and [22] is further investigated in this paper. Broadside radiation is possible with this new LWA design along with beam patterns that scan as a function of frequency from 19 to 26 GHz in the far-field. As shown in Fig. 1 the guiding surface is defined by a radial configuration of width-modulated microstrip lines printed on a GDS with transverse magnetic (TM) SWs generated by an arrangement of slots in the ground plane. In particular, this SW source [24], [25], or surface-wave launcher (SWL), is connected to a 50-Ω coplanar waveguide transmission line. A high relative dielectric constant is also used ($\varepsilon_r = 10.2$) to ensure efficient coupling into the dominant TM_0 SW mode of the slab [24], [25]. When SWs are incident onto the printed width-modulated microstrip lines, LWs can be excited with radial propagation along the 2-D antenna aperture.

Near the origin, as defined in Fig. 1, a transition section is also employed for the radially directed strips (see Fig. 2). Following the preliminary findings in [5], our new transition section, defined by a microstrip line (of width w_{min}) and four unit cells with increasing maximum line widths (w_{max}), can control

Manuscript received November 11, 2012; revised July 19, 2013; accepted July 22, 2013. Date of publication July 25, 2013; date of current version October 02, 2013.

S. K. Podilchak, A. P. Freundorfer, and Y. M. M. Antar are with the Electrical Engineering Departments of the Royal Military College of Canada (RMC) and Queen's University, Kingston, ON K7K 7B4, Canada (e-mail: skp@ieee.org).

L. Matekovits and M. Orefice are with the Department of Electronics and Telecommunications, Politecnico di Torino, 10129 Torino, Italy (e-mail: ladislau.matekovits@polito.it).

Color versions of one or more of the figures in this paper are available online at http://ieeexplore.ieee.org.

Digital Object Identifier 10.1109/TAP.2013.2274791

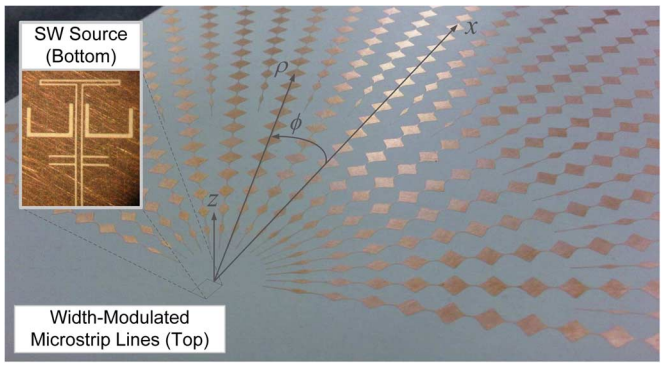

Fig. 1. Planar 2-D LWA investigated in this work. The cylindrical TM SW field distribution, generated from the SWL (printed on the bottom), is gradually transformed into LWs by the addition of the radially directed and width-modulated microstrip lines. Essentially, the SW power generated by the slot arrangement [25] delivers energy to the radiating strips for power leakage.

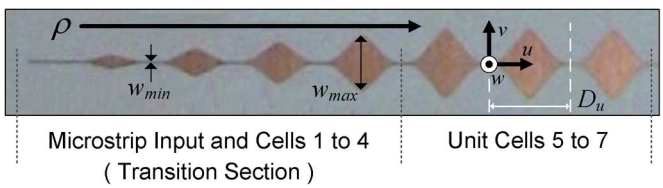

Fig. 2. A segment of one radially directed width-modulated microstrip line (near the origin). An array of these printed lines defines the antenna aperture.

the leakage rate while also reducing reflection losses of the antenna. More importantly, antenna efficiency can be improved by this transition section when compared to other SW driven LWA structures previously investigated by the authors [13], [16] and with no such width-modulated microstrip lines [9], [25]. For example, it will be shown that the radiation efficiency of the antenna in Fig. 1 is more than 85%. To the authors' knowledge, this is the first time that such a SW-fed LWA has been designed and measured, offering very good radiation performances, practical feeding, as well as ease of fabrication.

The radial antenna surface can be described as an array of unit cells and for simplicity its design is based on a 2-D model with periodicity in two orthogonal directions, u and v, as illustrated in Fig. 3. It will also be shown in the paper that such an adopted model may be a very good starting point for synthesis of the periodic structure that defines the 2-D antenna aperture, mainly since, the cylindrical SW phase front generated by the SWL is directed along the radial aperture or the longitudinal u-direction.

In Sections II and III we further describe the design of the LWA using a theoretically determined dispersion diagram (DD) for the periodic structure (Fig. 3). The theory needed for numerical generation of the DD will also be presented and the requirements for achieving radiation will be outlined. In addition, field plots of the non-modulated guide are provided in an effort to explain the coupling of SWs into the printed microstrip lines, i.e. TM SWs into microstrip. Implementation of the LWA is described in Section IV while the design of the transition section is detailed in Section V. Results are further supported by numerical calculations, full-wave simulations, and antenna measurements. Section VI provides a brief conclusion of the presented material while additional information, in support of the paper, has been prepared in the Appendix Sections.

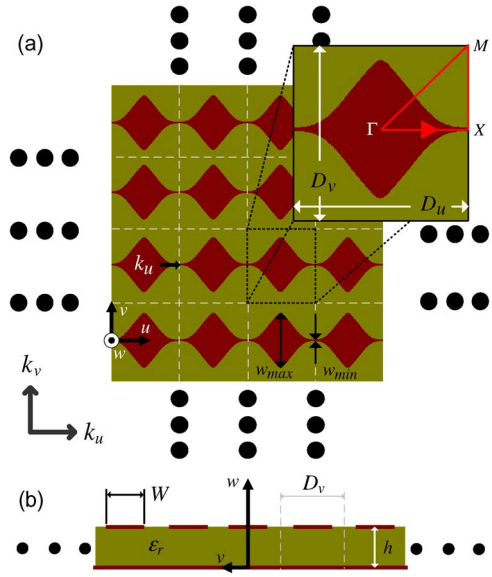

Fig. 3. (a): The 2-D antenna aperture can be modeled as a grid or array of unit cells with periodicity in the longitudinal and transverse directions, u and v, respectively with spatial periodicities D_u and D_v. (b): The unperturbed structure (no modulation), with constant microstrip line widths, W, can be defined as a transverse-periodic microstrip guide.

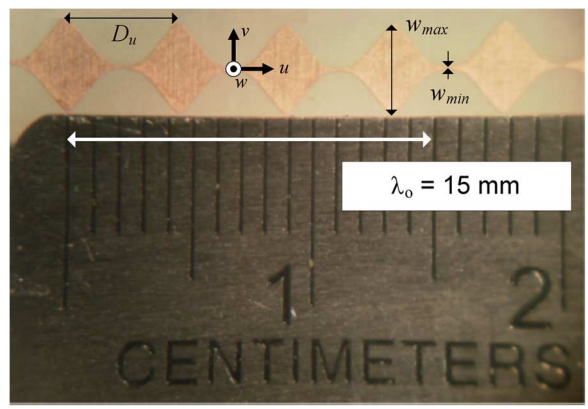

Fig. 4. Section of the periodic structure. The Nth unit cell is defined by the maximum and minimum widths, w_{max} and w_{min}, of the microstrip line. The free space wavelength, λ_0, is equivalent to 10 $D_u/3$ at 20 GHz.

II. Theoretical Considerations

By the width variation of such an array of microstrip lines (Figs. 3 and 4) the effective dielectric constant, ε_{eff}, can be sinusoidally modulated around an average value within the unit cell, ε_{avg}. Such a periodic variation can be thought to characterize the mechanism of controlled LW radiation and defines a SMRS [17]–[19]. This periodic structure is dependent on frequency, thickness h of the utilized GDS and its relative dielectric constant, ε_r, as well as the maximum and minimum widths (shape) of the microstrip line, respectively w_{max} and w_{min}, and spatial periodicities D_u and D_v of the unit cell.

The incident SWs generated from the slot source are perturbed when directed onto the SMRS and this causes the phase velocity of the guided waves to be periodically modulated due to the varying surface impedance. Furthermore, with knowledge of the complex longitudinal wavenumber, k_u, the nature of the far-field beam pattern can be determined. In comparison, when

SWs are directed onto a structure with no modulation (constant microstrip line width, W, with transverse periodicity D_v) perturbation still occurs, however, fields are bound defining a transverse-periodic microstrip guide with k_u real. Both these modulated and non-modulated microstrip guides will be analyzed in the paper.

A. Problem Formulation

Consider the propagation of an electromagnetic wave in a homogeneous and isotropic media. In a $v-w$ plane transverse to the direction of wave propagation, u, the electromagnetic wave can be decomposed into the sum of two field components: a transverse electric (TE) wave and a transverse magnetic (TM) wave. However, if the propagation media is no longer homogeneous, for example, when the effective permittivity or permeability for the structure under study becomes u-dependent, with $\varepsilon(u)$ or $\mu(u)$, determination of the eigenvalues is more involved. A width-modulated microstrip structure achieving controlled LW excitation, as investigated in this work, can be represented by such a periodic variation; $\varepsilon(u)=\varepsilon_{eff}(u)\varepsilon_0$, where $\varepsilon_{eff}(u)$ is the effective permittivity with u-dependence.

Now we will focus our attention on defining the field quantities for such a structure by applying periodic boundary conditions [26], [27], reviewing the dominant electromagnetic wave that propagates on a single microstrip transmission line [29], and investigating the fields that can be generated on a transverse-periodic microstrip guide due to an incident SW.

B. Periodic Material Analysis & Resulting Wave Equations

By studying 1-D variation along the u-direction with period D_u the Fourier expansions of the effective permittivity and permeability within the unit cell can be expressed in the most general form as

$$\varepsilon_{eff}(u)=\varepsilon_0\sum_{n=-\infty}^{\infty}\varepsilon_{r,n}e^{j\frac{2n\pi}{D_u}u}=\varepsilon_{avg}\varepsilon_{r,eff}(u)$$
$$\mu_{eff}(u)=\mu_0\sum_{n=-\infty}^{\infty}\mu_{r,n}e^{j\frac{2n\pi}{D_u}u}=\mu_{avg}\mu_{r,eff}(u) \quad (1)$$

where $\varepsilon_{r,n}$ and $\mu_{r,n}$ represent the coefficients of the n-th harmonic of the relevant quantities with respect to the free space values ε_0 and μ_0. In our LWA we limit variation to the effective permittivity, $\varepsilon_{eff}(u)$, and will consider the constant, free space value for the magnetic permeability, i.e. $\mu_{eff}(u)=\mu_0$ (a non-magnetic material).

Inserting (1) into Maxwell's Equations for the inhomogeneous medium, we have [22]:

$$\nabla_t^2E_t+k^2\varepsilon_{r,eff}(u)E_t=0 \quad (2)$$
$$\nabla_t^2H_t+k^2\varepsilon_{r,eff}(u)H_t-\frac{1}{\varepsilon_{eff}(u)}\frac{\partial\varepsilon_{eff}(u)}{\partial u}\frac{\partial H_t}{\partial u}=0 \quad (3)$$

where the subscript t denotes the components transverse to the direction of propagation and the electric (E) and magnetic (H) field quantities relate to the TE and TM waves respectively. The term ∇_t is the transverse component of the differential operator, ∇, and $k=\sqrt{\varepsilon_{avg}}k_0$ is the wavenumber in the considered (unbounded) media. Moreover, k_u (see Fig. 3) denotes the longitudinal component along the u-direction with $k_u=\sqrt{k^2-k_t^2}$ and where k_t defines the wavenumber in the transverse plane.

Sinusoidal variation of the effective permittivity can be achieved if we limit the expansion in (1) to the first three terms, $n=-1$, 0, 1 (with $\varepsilon_{r,n}=0$ otherwise), and after further considering $\varepsilon_{r,-1}=\varepsilon_{r,1}$ and denoting $2\varepsilon_{r,1}/\varepsilon_{r,0}\equiv M_u$ as the modulation index, we have

$$\varepsilon_{eff}(u)=\varepsilon_{avg}\left(1+M_u\cos\frac{2\pi}{D_u}u\right)$$
$$\text{with}\quad \varepsilon_{r,eff}(u)\equiv 1+M_u\cos\frac{2\pi}{D_u}u. \quad (4)$$

It should also be noted that in the absence of modulation, $\varepsilon_{eff}(u)=\varepsilon_{avg}$ giving $\partial\varepsilon_{eff}(u)/\partial u=0$. This results in (2) and (3) reducing to wave propagation in an isotropic and homogeneous media.

It is interesting to differentiate (4) with respect to u and insert the result back into the developed wave equation for the TM case, (3). After some manipulations we get

$$\nabla_t^2H_t+k^2\varepsilon_{r,eff}(u)H_t+K(u)\frac{\partial H_t}{\partial u}=0$$
$$\text{with}\quad K(u)=M_u\frac{2\pi}{D_u}\frac{\sin\frac{2\pi}{D_u}u}{1+M_u\cos\frac{2\pi}{D_u}u}. \quad (5)$$

For small modulation index values, i.e. when $M_u\ll 1$, $K(u)$ can be approximated by $M_u(2\pi/D_u)\sin(2\pi/D_u)u$, and when only maximum values are considered for the $\sin(\cdot)$ term, $K(u)\cong M_u(2\pi/D_u)$. This $K(u)$ term is also normalized by the factor $D_u/2\pi$ over the longitudinal length of the unit cell; i.e. the spatial periodicity, D_u. Moreover, when the variation of the transverse magnetic field, H_t, is small across the unit cell, the $\partial H_t/\partial u$ term can be thought of as negligible when compared to the other field quantities in (3). This results in $K(u)(\partial H_t/\partial u)\ll\nabla_t^2H_t+k^2\varepsilon_{r,eff}(u)H_t$, making the solution of (5) to be of similar form to (2), the TE case. This approximation may be appropriate as the length of the free-space wavelength is about 3.5 unit cells (see Fig. 4) when considered over the operating bandwidth (BW) of the LWA design. Further explanations on this approximation is discussed in Appendix I where the generated current distributions on the width-modulated microstrip lines are examined.

C. Field Analysis of the Fundamental Microstrip Mode

The electromagnetic wave that propagates on a single, non-radiating and non-modulated (constant width) microstrip transmission line involves both a TE and TM wave part [29]–[32]. More specifically, the field components for microstrip involve a hybrid coupling of both TM and TE modes, and due to the frequency dependent solution and propagation within the dielectric and air regions, a true transverse electromagnetic (TEM) wave cannot be supported at high frequencies. This hybrid wave is classically described as quasi-TEM with wave propagation defined by the effective dielectric constant.

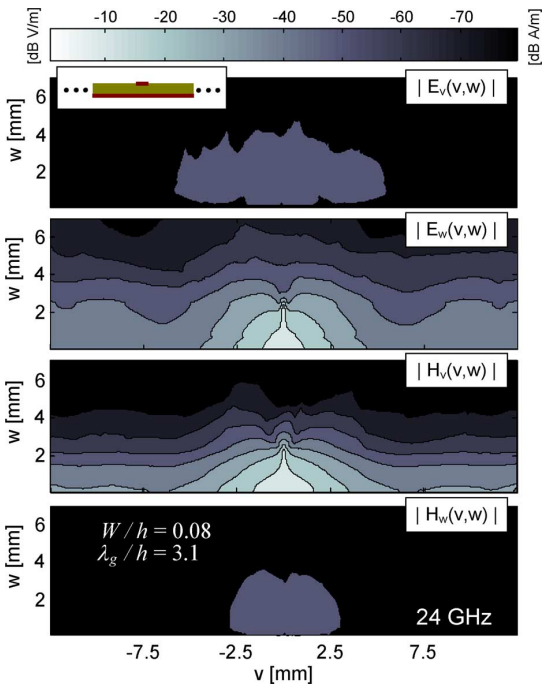

Fig. 5. Simulated[1] electric and magnetic field distribution for microstrip ($W = 0.1$ mm) for the GDS employed within the antenna structure. Values normalized to the observed maximum for E_w and H_v, respectively. It can be observed that the TM field components dominate the transverse plane.

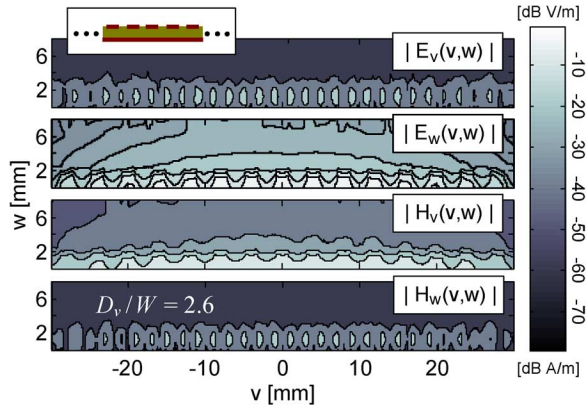

Fig. 6. Simulated[1] field distribution for the transverse periodic microstrip guide generated by an incident TM SW (with a TM_0 SW mode field configuration[2]) at 24 GHz for $\varepsilon_r = 10.2$, $D_v/h = 3.1$, and $D_v/W = 2.6$ with $D_v = 4$ mm. Values normalized to the observed maximum for the excited fields within the guide and with E_w and H_v respectively dominant. It can be observed that a hybrid-mode of both TM and TE waves propagates within the structure (E_v, E_w, H_v, and H_w defining quasi-TEM).

For example, observe the simulated field distribution[1] in Fig. 5 for a microstrip transmission line at 24 GHz printed on the GDS employed for the investigated structure ($h = 1.27$ mm and $\varepsilon_r = 10.2$). The dominant field terms are E_w and H_v in the transverse plane for the microstrip guide with such an electrically thick substrate (defined here as $\lambda_g/h = 3.1$ where $\lambda_g = \lambda_0/\sqrt{\varepsilon_r}$). In fact, these E_w and H_v field terms define the TM part for the wave propagating along the transmission line. This suggests that the incident TM waves generated by the slot source at the origin can couple into microstrip. Physically, the field lines of the quasi-TEM microstrip line are aligned with that of the TM_0 SW mode of the slab. A parallel-plate-type microstrip mode [29]–[32] may also be representative for this slab and strip topology. This implies that field terms that propagate on microstrip for this GDS are similar to a parallel-plate mode of operation (of finite width) as the majority of the fields are contained within the slab region.

D. Field Analysis of the Non-Modulated Guiding Structure

A similar analysis can be extended to the host guiding structure, defined by an array of parallel microstrip lines, with no modulation (see Fig. 3(b)). The electric and magnetic field distributions can also be simulated[2] as shown in Fig. 6, where a hybrid-mode of both TM and TE waves propagate within the unperturbed structure. This is in contrast to the single microstrip line in Fig. 5 which is mostly dominated by TM fields (E_w and H_v). These results imply that the field solutions obtained for TE waves on microstrip, in particular the solutions found for the wave equation in (2) for the TE case, can provide indication of the field behavior for TM waves as well. This is due to the fact that field propagation along the unperturbed transverse-periodic microstrip guide, when incident with TM SWs (which are generated by the SWL), is a hybrid coupling of both TM and TE waves which defines a quasi-TEM mode. The dispersive behavior of these guides are further examined in Appendix II.

E. General Discussion

With the aforementioned design factors in mind, mainly that M_u should be small ($M_u \ll 1$), the length of the periodic unit cell should be made small with respect to the free space wavelength, λ_0, and that good coupling can occur into the dominant mode of the guiding structure (excited by the SWL), field solutions for the TE case as well as the forthcoming DD can provide indication of the related quasi-TEM guide, and perhaps, at least a first order approximation to the problem. In the next section we will focus our attention on this TE case. Solutions and explanations thereof will be provided using Mathieu's functions, in an effort to develop the DD for the unit cell within the LWA structure, and also under the assumption that $K(u)(\partial H_t/\partial u) \ll \nabla_t^2 H_t + k^2 \varepsilon_{r,eff}(u) H_t$.

[1]It should be mentioned that a minor asymmetry can be observed in the simulated field plots shown in Figs. 5 and 6. This effect can be attributed to the given precision of the commercial simulator, HFSS [28]; results were analyzed after two consecutive iterations with a 2% convergence error or less. These same error bounds were established for all full-wave simulations reported in this work, which included the SW source and the width-modulated microstrip lines. Increased accuracy was not feasible due to the computational requirements of such electrically large and complex structures.

[2]In these simulations [28] a uniform SW field distribution (TM_0 SW mode) with no variation in the v-direction ($\partial H_v/\partial v \approx 0$) was generated at the origin and then incident upon the 2-D grid of non-modulated lines. The guide started at $u = 10$ mm and extended to infinity. The field plots in Fig. 6 are provided in a transverse plane at $u = 30$ mm. A hybrid-mode of both TM and TE waves propagate within the structure defining a quasi-TEM mode.

III. Unit Cell Synthesis by Mathieu's Equations

Let us start with a general description of the Mathieu's equations [33]–[37], and their solution in terms of Mathieu's functions. Initially, the classical development of the formulation of the problem is reviewed. This assists in the understanding of our developed closed form equations that are used to compute the DD.

Consider the two dimensional Helmholtz equation for the general field component $U(u,v)$ in the 2-D reference system,

$$\frac{\partial^2 U}{\partial u^2}+\frac{\partial^2 U}{\partial v^2}+k^2U=0, \tag{6}$$

with unit vectors $\hat{u}$ and $\hat{v}$, for the unit cell (as outlined in Fig. 3) and with (6) representing wave propagation for the ensemble 2-D periodic structure. Now transforming the reference system into an elliptical coordinate system with foci $\pm\tau$ and with $u=\tau\cosh\xi\cos\eta$ and $v=\tau\sinh\xi\sin\eta$ for $\xi\in[0,\infty)$ and $\eta\in[0,2\pi)$, respectively, (6) becomes

$$\frac{d^2\Phi}{d\eta^2}+(a-2q\cos 2\eta)\Phi=0 \tag{7}$$

$$\frac{d^2R}{d\xi^2}-(a-2q\cosh 2\xi)R=0. \tag{8}$$

Moreover, a solution of the form $U(\xi,\eta)=R(\xi)\Phi(\eta)$ can be obtained, where $q=(\tau^2k^2/4)$ and a is the separation constant arising from the separation of variables (both these constants, a and q, will be further defined in Section III-A for the investigated unit cell). These second order differential equations in (7) and (8) are respectively known as ordinary and modified Mathieu's equations [33]–[37].

A. Application to the Considered Periodic Structure

In the case of an electromagnetic wave propagating in the periodic structure along the u-direction, (2) can be expressed as

$$\frac{d^2\Phi}{du^2}+\omega^2P(u)\Phi=0 \tag{9}$$

where $\omega=2\pi f$ and $P(u)=\varepsilon_0\mu_o\varepsilon_{eff}(u)$ is a periodic function with periodicity D_u. Now after introducing $\eta=\pi u/D_u$, and after some substitutions, we get

$$\frac{d^2\Phi}{d\eta^2}+(a+2q\cos 2\eta)\Phi=0 \tag{10}$$

with $a=\varepsilon_{avg}(D_uk_0/\pi)^2$ and $q=\varepsilon_{avg}M_u(D_uk_0/\pi)^2/2=aM_u/2$. Using this representation and transforming the periodicity from D_u to π, (9) is now of similar form to the ordinary Mathieu differential equation (7).

The dispersive behavior of interest corresponds to the phase constant of the complex parameter κ and the resulting spatial harmonics where $\kappa_n=\kappa+(2n\pi/D_u)\equiv k_u$. Physically speaking, we are interested in the resulting phase advance in the u-direction across the unit cell, $\beta_u(\approx \mathrm{Re}\{\kappa_n\})$, with the $n=-1$ harmonic corresponding to Bragg radiation of the incident SWs. This harmonic is a spatial mode that can radiate whenever $-k_0<\beta_u<k_0$. More specifically, we are interested in the resulting pointing angle θ_p of the far-field beam pattern that can be generated by this radiating LW mode, since $\theta_p\approx\sin^{-1}(\beta_u/k_0)=\sin^{-1}(\hat{\beta}_u)$.

Following [19] the LW attenuation constant, $\alpha\approx-\mathrm{Im}\{\kappa\}$, can also be determined by taking into consideration the $n=0$ and $n=-1$ spatial harmonics, where

$$\hat{\alpha}=\frac{\alpha}{k_0}=\mathrm{Im}\left\{\left(\varepsilon_{avg}\frac{M_u}{4}\right)^2\frac{\frac{1}{\sqrt{\varepsilon_{avg}}(\varepsilon_{avg}-1)}}{\frac{1-j\hat{k}_{t,air}}{\sqrt{\varepsilon_{avg}-1}}}\right\}$$

and

$$\hat{k}_{t,air}=\frac{k_{t,air}}{k_0}=\sqrt{\frac{1-\left(\beta_u-\frac{2\pi}{D_u}\right)^2}{k_0^2}} \tag{11}$$

with $\hat{k}_{t,air}$ defining the complex transverse wavenumber in the air region (for the $n=-1$ spatial harmonic). Equation (11) is a valid approximation when the pointing angle is defined in the backward or forward radiating regions for reduced modulation values [19], however, additional harmonics (terms) are required to accurately describe the antenna leakage at broadside as well as in the backward and forward end-fire directions.

To calculate the DD, both integer and non-integer Mathieu's functions [34]–[37] are required; results are shown in Fig. 7. Considering the definition of M_u in (4) and (10), we have $a=2q/M_u$, and therefore using an (a,q) basis grid, the modulation term M_u corresponds to the slope of a straight line. In particular, two lines are plotted in Fig. 7 with $M_u=0.2$ and 0.8. Their intersections points (at coordinates a_i,q_i) allows one to determine the propagation characteristics within the unit cell for the defined modulation; i.e. β_u for $M_u=0.2$ or $M_u=0.8$. In particular, these intersection points[3] can be calculated using a standard null searching algorithm (see [5] and [22]) where β_u can be determined on the border of the stability zones (stopbands), or their combination inside the passbands.

In the absence of modulation the oblique line with slope M_u in Fig. 7 reverts to the horizontal a-axis ($q\equiv 0$) and therefore no stop-bands exist with the lower band-limit of the first stop-band going to infinity; i.e. fields are bound defining the transverse-periodic microstrip guide with no modulation where the fundamental (non-radiating) mode of the structure exists with the limits of the first irreducible Brillouin zone extending to infinity. This is because the longitudinal periodicity of the unit cell, D_u, has an undefined length.

B. Unit Cell Synthesis & Implementation

Following the results of the previous sections the theoretical DD can be calculated numerically. As a starting point we choose our periodic structure to exhibit stop band characteristics above the operating frequency of the directive SW source (≈23 GHz

[3]Intersections of the integer order functions (continuous lines) in Fig. 7 correspond to these stopband band-limits, while those with non-integer order functions (dashed lines) allows one to determine the dispersion relations for the given mode. These different zones can be observed on the graph and are delimited by the integer order functions labeled $Ce_\nu(\eta,q)$ and $Se_\nu(\eta,q)$. For instance, the shaded gray regions between $Ce_\nu(\eta,q)$ and $Se_\nu(\eta,q)$ of the same order ν, correspond to the calculated stop band zones [17]–[19]. In particular, the red and green continuous lines, relating to $Ce_1(\eta,q)$ and $Se_1(\eta,q)$, can respectively define the boundary for the first stop band of the width-modulated transverse-periodic microstrip guide. Moreover, the shaded gray region bounded by the continuous curves with the same subscript, for example, the continuous purple and cyan curves, $Ce_2(\eta,q)$ and $Se_2(\eta,q)$, relate to the second stop band of the modulated guide. This zone corresponds to the open LW stopband [11], [12] for the radiating $n=-1$ spatial harmonic.

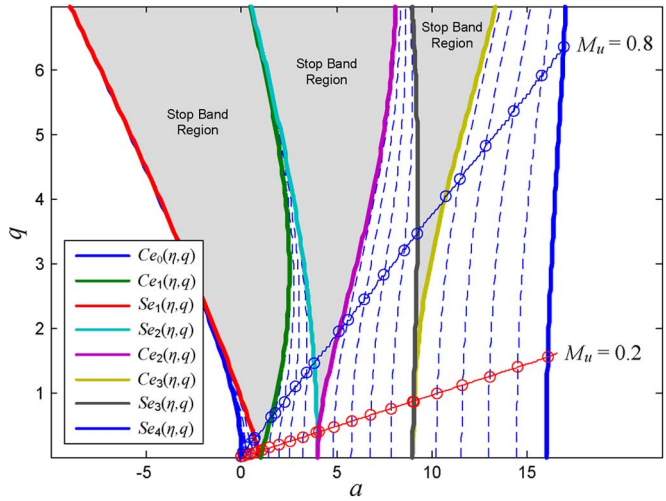

Fig. 7. A collection of Mathieu functions (of order ν) for integer (continuous line) and non-integer (dashed line) values. The gray shaded regions, between the Mathieu functions of the same order, are representative of the frequency stop band regions for the periodic structure.

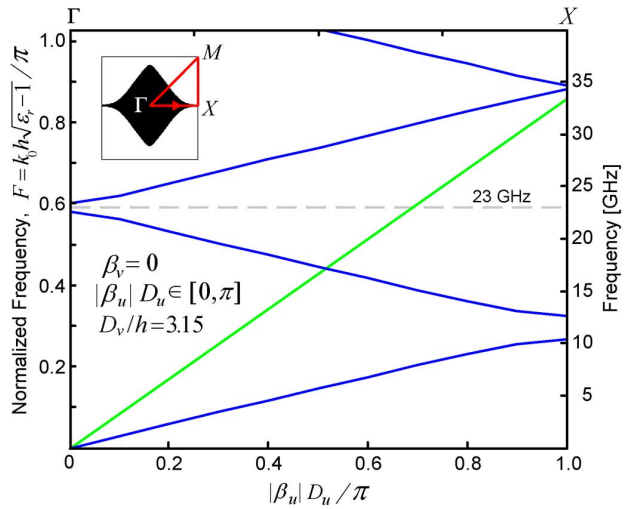

Fig. 8. Calculated dispersion diagram for the Nth unit cell along the u-direction. This also corresponds to the dispersion diagram for the guided waves along the radial aperture. The light-line, $\beta_u = k_0$, is represented with a solid green line with radiation of the $n = -1$ spatial harmonic occurring from about 17 to 35 GHz or from $-k_0 < \beta_u < k_0$. The open LW stopband can be observed from 22.6 GHz to 23.4 GHz.

[25]) with LW radiation [10]–[12] occurring above the light line (defined here when $\beta_u/k_0 = 1$) for the $n = -1$ spatial harmonic. Furthermore, frequency beam scanning is desired from backfire (at about 18 GHz) through broadside (with radiation in an open LW stopband [12] beyond 23 GHz) along with continued beam scanning in the forward direction.

It should also be mentioned that M_u does not substantially modify the position of the LW stopband region but can control the upper and lower band limits (or frequency BW) of the band stop region. This can be observed in Fig. 7 for $M_u = 0.8$ and $M_u = 0.2$. In fact, the position of the LW stopband is mainly controlled by ε_{avg} and D_u. With these factors in mind M_u should also be small ($M_u \ll 1$) as discussed in Section II. This is desired to ensure that the upper and lower band limits for each stopband region are not largely spaced with respect to frequency. For example and as a design goal, we choose the modulation scheme such that the BW of the band gaps are less than 1 GHz in frequency. In addition, a reduced BW is also desired for the radiating $n = -1$ mode in the open LW stopband. This can minimize the effect of reduced antenna gain, which can be observed for typical 2-D planar-periodic LWAs [9] when radiating at broadside through the $n = -1$ harmonic. Moreover, our design approach is not to eliminate the effects of the open-stopband region, but rather, to design a unit cell with a reduced bandgap. Other strategies to minimize the negative effects in the open-stopband region have also been investigated in [38]–[40] for 1-D LWAs which achieve leakage by the $n = -1$ and $n = 0$ spatial harmonics.

Given these desired characteristics the unit cell can be synthesized accordingly. To ensure functionality with the employed SWL, substrate properties were first fixed to a thickness h of 1.27 mm and a relative dielectric constant ε_r of 10.2 [25]. These values were previously found to allow for efficient coupling into the dominant TM_0 SW mode of the slab [24] by the SWL. Thus antenna operation is to be established within the frequency band where the planar SW feed can efficiently couple power into the GDS [25].

With this in mind, the DD can be computed for the investigated periodic structure as shown in Fig. 8. Here by setting $D_u = 4.5$ mm, $D_v = 4.0$ mm, $\varepsilon_{avg} = 8.6$, $\varepsilon_r = 10.2$, and $M_u = 0.2$ we are able to achieve the center frequency for the open LW stopband region to be positioned at around 23 GHz with a BW of about 0.8 GHz. Now using the result of [22] in that $\varepsilon_{avg} = (\varepsilon_{eff,min} + \varepsilon_{eff,max})/2$, the required minimum and maximum effective dielectric constant values ($\varepsilon_{eff,min}$ and $\varepsilon_{eff,max}$) need to be determined while simultaneously maintaining a small value for the modulation factor, M_u, mainly that, $M_u = (\varepsilon_{eff,max} - \varepsilon_{eff,min})/2\varepsilon_{avg}$. We complete this task using a commercial eigenmode solver (CST [41]), mainly, to determine the maximum and minimum strip-width values to achieve the needed field perturbation within the unit cell, while also considering the effect of the transverse periodicity present in the 2-D structure [42].

Results are plotted versus the strip-width to substrate thickness ratio, W/h, in Fig. 9 for the transverse-periodic microstrip guide. Values are also compared to calculated effective dielectric constant values for a common microstrip guide (considering quasi-TEM propagation[4]) and a parallel-plate guide[5] ($W = D_v$). As expected the effective dielectric constant of the transverse-periodic microstrip guide, which is also related to the normalized phase propagation constant $\hat{\beta}(= \sqrt{\epsilon_{eff}} = \beta/k_0)$, approaches ε_r as the strip-width extends to the transverse periodicity $D_v(= 4.0$ mm$)$. This is because the fields are mostly contained within the dielectric for the nearly closed structure

[4]In our analysis we calculate ε_{eff} for the fundamental quasi-TEM mode of microstrip using the well known equation:

$$\varepsilon_{eff} = \begin{cases} \frac{\varepsilon_r+1}{2} + \frac{\varepsilon_r-1}{2} \\ \quad \times \left[\left(1+\frac{12h}{W}\right)^{-\frac{1}{2}} + 0.04\left(1-\frac{W}{h}\right)^2\right], & \frac{W}{h} < 1 \\ \frac{\varepsilon_r+1}{2} + \frac{\varepsilon_r-1}{2}\left(1+\frac{12h}{W}\right)^{-\frac{1}{2}}, & \frac{W}{h} > 1. \end{cases}$$

[5]The fundamental TM_0 mode for parallel-plate with $\varepsilon_{eff} = \varepsilon_r$ and $\beta = \sqrt{\varepsilon_r} k_0$ can propagate at all frequencies due its zero cutoff frequency. In addition, the TM_0 mode of parallel-plate is actually a TEM wave due to its resulting field configuration.

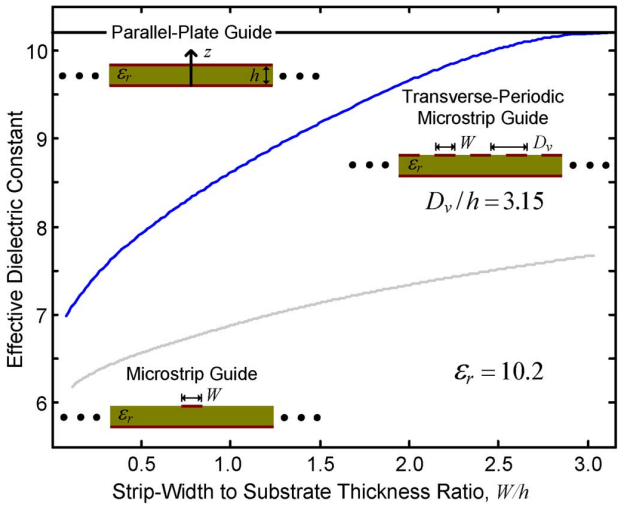

Fig. 9. The effective dielectric constant versus the strip-width to substrate thickness ratio, W/h, for the fundamental mode of parallel-plate (calculated, black line), for the transverse-periodic microstrip guide (simulated, blue line), and for quasi-TEM microstrip (calculated, grey line). The effective dielectric constant for the transverse-periodic microstrip guide resembles the parallel-plate mode when $W \rightarrow D_v$ (or exactly when $W/h = 3.15$).

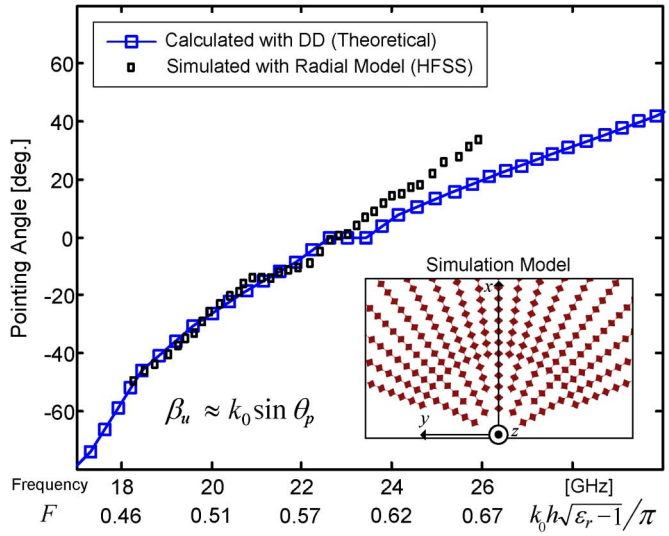

Fig. 10. Calculated pointing angle using the dispersion diagram for the Nth unit cell in Fig. 8. Agreement can be observed with the corresponding radial structure [16] (no transition section and driven by a directive SWL [25] placed at the origin). This simulated LWA structure is shown in the figure inset.

with reduced gaps between the microstrip lines, defining a parallel-plate like mode.

For the synthesis of the Nth cell, with $D_u/D_v = 1.125$, we select the minimum [maximum] microstrip line width to be 0.1 mm [3.7 mm], mainly by inspecting the results plotted in Fig. 9 for transverse-periodic microstrip guide and by making use of the desired DD in Fig. 8. It should also be noted that the transverse dimension, D_v, plays an important role in determining the desired minimum and maximum values for the effective dielectric constant [42] as well as to ensure good phase matching (see Fig. 21) with the incident SWs from the SWL. For instance, if the separation between the parallel microstrip lines was reduced $(W/h > 2.9)$, the transverse microstrip guide would act as a closed parallel-plate guide with reduced SW coupling and consequently increased reflections. As a result of this design approach, we select the unit cell parameters as follows: $\varepsilon_{eff,min} = 6.982$, $\varepsilon_{eff,max} = 10.19$, and $M_u = 0.1867$.

C. Unit Cell Verification

To confirm the engineering approach to the unit cell, calculated pointing angles are compared in Fig. 10 to those for a radial LWA structure using the SWL positioned at the origin [16] and with no transition section. Simulated θ_p values using HFSS [28] are in close agreement with those calculated by the DD in Fig. 8 and these results suggest that the preliminary assumptions (grid or array of unit cells defining the 2-D periodic structure, as in Fig. 3) are indeed a valid engineering starting point to the problem. Mainly that, the developed DD can assist with the synthesis of the unit cell.

Good agreement is shown in Fig. 10 from 18 to 23 GHz. However, it should be noted that there is a slight discrepancy between the pointing angles calculated using the DD (Fig. 8) and the results for the radial simulation model (Fig. 10 inset). This divergence, which is further examined and explained in Appendix II, can be observed for frequencies beyond 23 GHz (or $F > 0.6$) with deviations in the calculated and simulated pointing angles

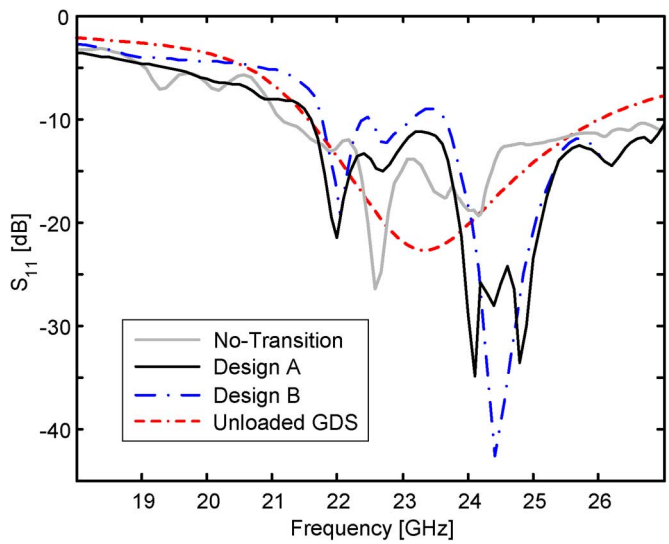

Fig. 11. Simulated reflection coefficient for the radial topology with no transition section; i.e. the planar LWA shown in the inset of Fig. 10 with a directive SWL as the antenna feed [16]. Results are also compared to the simulated values for Design A and Design B (Fig. 12) as well as an unloaded GDS (air-dielectric interface with no top strips). All structures are fed by a directive SWL [25]. It can be observed that improved 50-Ω antenna matching can be obtained with Designs A and B due to the added transition sections.

approaching 13° at 26 GHz. It should also be mentioned that this simulated LWA exhibits poor matching below and above 18 and 24 GHz (see Fig. 11) and thus no distinct beam patterns are observed in the far-field for comparison with the theoretical. This limited beam scanning range is related to the operational BW of the SWL, which is about 21 to 26 GHz [25] as also shown in Fig. 11. Nevertheless, agreement is observed in the calculated and simulated pointing angles.

IV. Antenna Designs & Layout Implementation

Using the principles for synthesis of the unit cell two LWA designs were considered. Designs A and B as shown in Fig. 12.

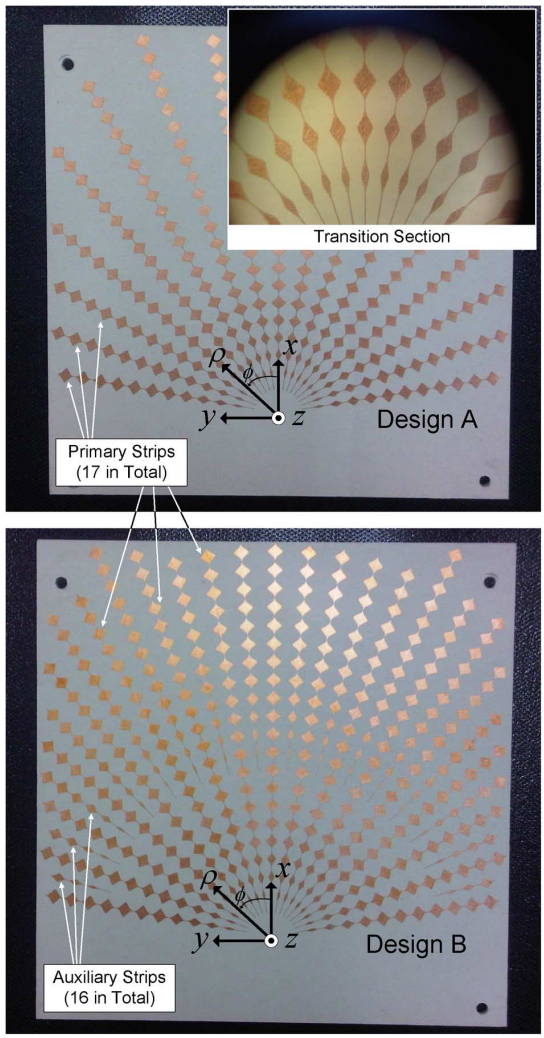

Fig. 12. Investigated LWAs Design A and Design B. The transition section near the origin (Fig. 13) is shown in the first figure inset. Designs A utilized a total of 17 primary width-modulated printed microstrip lines for LW excitation. For comparison Design B (also shown in Fig. 1) employed 33 radial strips, and as expected, improved radiation efficiencies were observed, mainly due to the auxiliary width-modulated microstrip lines for Design B.

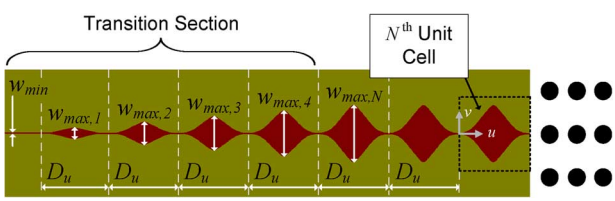

Fig. 13. Sequence of the first seven unit cells of the width-modulated microstrip line designed for controlled leakage. Dimensions are as follows: $D_u = 4.5$, $w_{min} = 0.1$, $w_{max,1} = 0.7$, $w_{max,2} = 1.5$, $w_{max,3} = 2.2$, $w_{max,4} = 3.0$, and $w_{max,N} = 3.7$ (all values in mm) where $w_{max,N}$ defines the microstrip width for the Nth unit cell within the periodic structure.

It should be mentioned that Design B was previously shown in Fig. 1, while in this section, we provide important details regarding placement of the radial strips and transition section (Fig. 13). Specifically, our implementation procedure for the guiding surface of the LWAs is summarized.

A standard substrate size of 12 cm by 12 cm was employed using the aforementioned guiding structure (Rogers Corporation 6010.2LM GDS: $\varepsilon_r = 10.2$, $h = 1.27$ mm, and $\tan\delta = 0.0023$). For Design A, the primary width-modulated strips were radially placed every 10° on the air-dielectric interface at a distance of 6.2 mm from the origin and starting with the transition section as shown in Fig. 2. The length of the strips, defined by the number of unit cells or spatial periodicity D_u, extended to the edge of the board. Thus a total of 17 radially directed, width-modulated microstrip lines were placed on top of the air-dielectric interface.

Following the layout procedure for Design A, the implementation of the second LWA (Design B) was very similar except for the additional auxiliary strips as shown in Fig. 12. More specifically, these 16 auxiliary strips were radially placed every 10° at a distance of about 10 unit cells from the origin and in the regions were no primary strips were present. Similar to the primary strips in Design A, these auxiliary strips extended to the edge of the grounded slab for Design B.

It will be shown in the next section that these auxiliary strips can improve the radiation efficiency of Design B when compared to Design A, mainly due to the increased number of radiating elements within the same physical aperture size. Moreover, since the orientation of the printed strips is radial, a uniform and relatively large current distribution (with respect to the free-space wavelength) is expected for these LWA designs with directive beam patterns in the far-field. Simulations of these current distributions are presented in Appendix I.

V. The Transition Section, Antenna Simulations, Measurements & Discussions

At this stage we outline the employed transition section and important details regarding its design. Numerical results and full-wave HFSS simulations [28] are reported in Figs. 14 and 15 as well as Table I. Measurements of the considered LWAs were completed in a calibrated anechoic chamber and agreement is observed with the simulations as shown in Figs. 16–19.

A. Theoretical Considerations

One important aspect for practical LWAs is to achieve a uniform aperture distribution, in that the antenna surface is to be engineered in such a way to ensure that the radiating elements leak the same amount of power as a function of distance from the origin. This can be challenging to achieve in practice. One particular solution is to design for a specified aperture illumination, a Taylor distribution as discussed in [6], where the LW attenuation constant, α, is non-constant over the radiating surface but is related by its position from the antenna source; i.e. α is a function of x, or in our example, $\alpha(\rho)$.

B. Design Principles of the Transition Section

The first four unit cells of the radially directed width-modulated microstrip lines (Figs. 2 and 13) were designed to achieve gradual LW radiation of the bound cylindrical SWs generated from the SWL. This is unlike the radial LWA design in [16] with no such control of the aperture illumination. In particular, by slowly increasing the width of the microstrip lines as a function of distance from the origin (for Designs A and B) a controlled aperture distribution was achieved were the phase velocity of the incident TM SWs observe a reduced perturbation within the transition section when compared to the remaining periodic structure. For instance, the first two unit cells of the

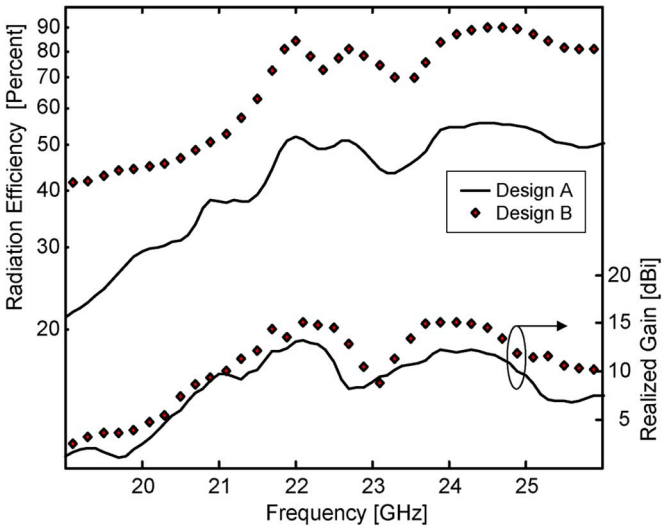

Fig. 14. Simulated radiation efficiency and realized gain in the $\mathrm{E}(x-z)$ plane for the complete antenna structures (feedline, substrate losses, width-modulated lines, and SWL as shown in Fig. 12). The reduction in radiated power at approximately 23 GHz corresponds to the open LW bandgap for broadside radiating frequencies. Radiation efficiency values were determined by comparing the maximum value of the realized antenna gain (which includes antenna mismatches) with respect to the pattern directivity of the main beam pattern in the $\mathrm{E}(x-z)$ plane using HFSS.

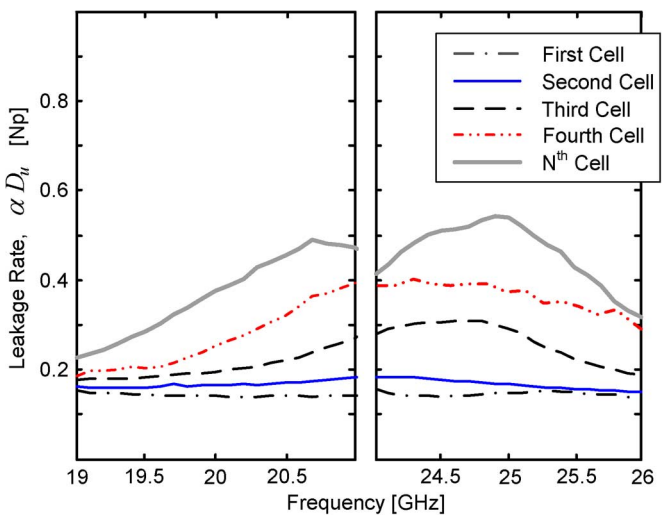

Fig. 15. Simulated leakage rate within the transition section and remaining Nth cells for backward [forward] radiating frequencies with $\theta_p < 0°$ [$\theta_p > 0°$] for 19 to 21 GHz [24 to 26 GHz]. The leakage rate was approximated from simulated far-field data by observing the half-power beamwidth, $\mathrm{BW}_{3\ \mathrm{dB}}$, of the radiated beam pattern as a function of frequency. Note: non-broadside radiating frequencies are shown since the leakage rate or $\mathrm{BW}_{3\ \mathrm{dB}}$ estimation is fairly accurate for non-broadside radiating angles [6], [10].

TABLE I
THEORETICAL OPEN STOPBAND REGION CORRESPONDING TO BROADSIDE RADIATING FREQUENCIES

Cell Number	Center Frequency	Bandwidth	Modulation
1st	$1.98/\pi$ [24.38]	$0.01/\pi$ [0.11]	$M_u = 0.0677$
2nd	$1.92/\pi$ [23.81]	$0.03/\pi$ [0.32]	$M_u = 0.1166$
3rd	$1.89/\pi$ [23.45]	$0.04/\pi$ [0.52]	$M_u = 0.1479$
4th	$1.87/\pi$ [23.15]	$0.06/\pi$ [0.71]	$M_u = 0.1744$
N^{th}	$1.86/\pi$ [23.01]	$0.07/\pi$ [0.81]	$M_u = 0.1867$

Note: Frequency values shown as $F = k_0 h\sqrt{\varepsilon_r - 1}/\pi$ [and in GHz]. Modulation factors, M_u, calculated for the respective unit cell.

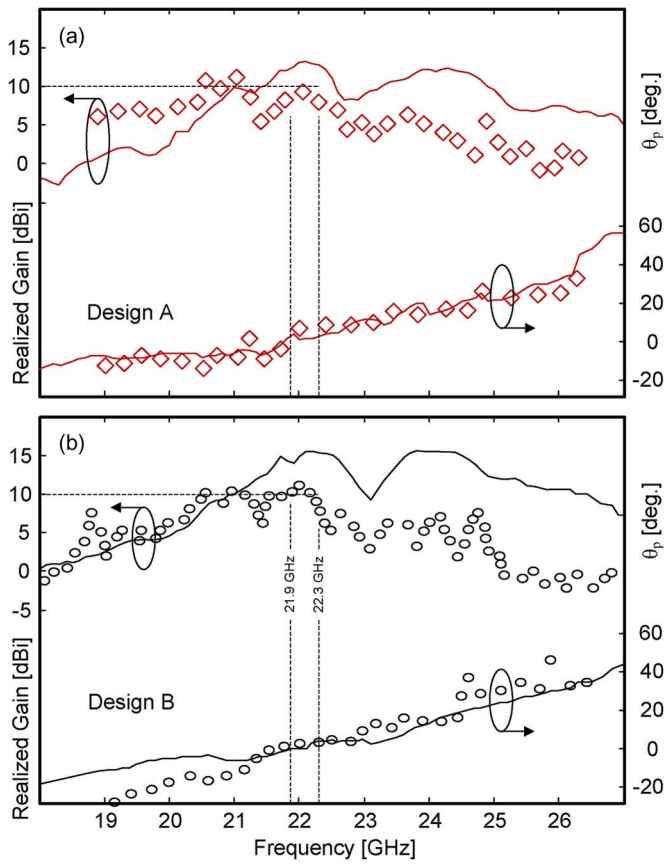

Fig. 16. Measurements (red $\diamond$/black $\circ$) and full-wave simulations (red/black lines) of the maximum realized gain and pointing angle (θ_p) in the $\mathrm{E}(x-z)$ plane as a function of frequency for Designs A and B. Cross-polarization levels (not shown) are less than 10 dB from the co-polarized maximum.

transition section have reduced modulation ($M_u \leq 0.12$ with $w_{max} \leq 1.5$ mm) when compared to the Nth unit cell ($M_u = 0.1867$).

C. Improved Antenna Operation Due to the Transition Section

The effect of this reduced perturbation near the origin serves two purposes. It improves the 50-Ω antenna match as SW reflections are minimized when incident onto the transverse-periodic microstrip guide, while also, slowly increasing the leakage rate as a function of distance from the origin. Different transition sections were investigated having other unit cell widths, but the presented topology (see Fig. 13) using four width modulated cells and a non-modulated microstrip line of length $D_u/2$ offered the best result in terms of good antenna matching, increased antenna gain, as well as design simplicity.

The simulated reflection coefficient is shown in Fig. 11 for Design A and Design B. It can be observed that the considered LWA designs offers a very good 50-Ω match when compared other SW driven structures. For example, $|S_{11}| < -25$ dB for both Design A and Design B from 24 to 25 GHz, while it is between -10 dB and -20 dB in this same range for the LWA

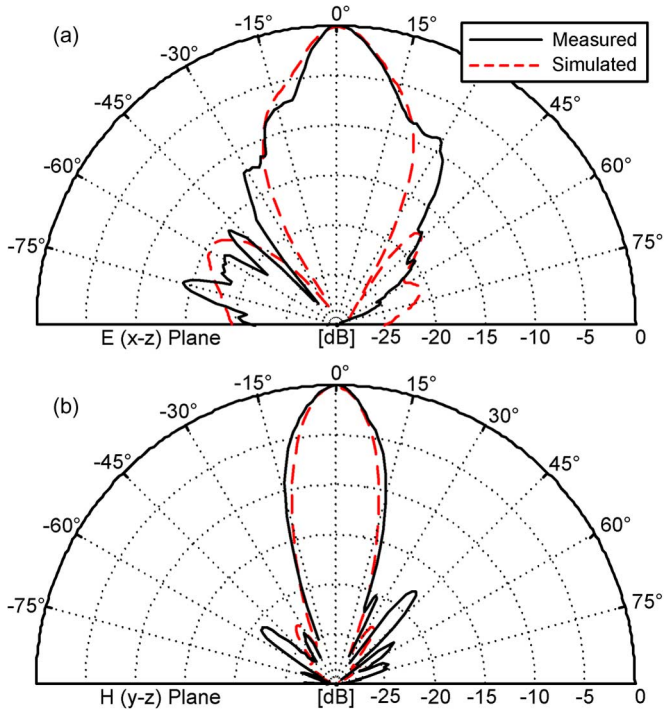

Fig. 17. Broadside beam patterns for Design B (E/H planes referenced to the main slot of the SWL). (a) $E_\theta(\phi = 0°)$. (b) $E_\phi(\phi = 90°)$. Measured [simulated] beam patterns shown at 21.5 [22.1] GHz.

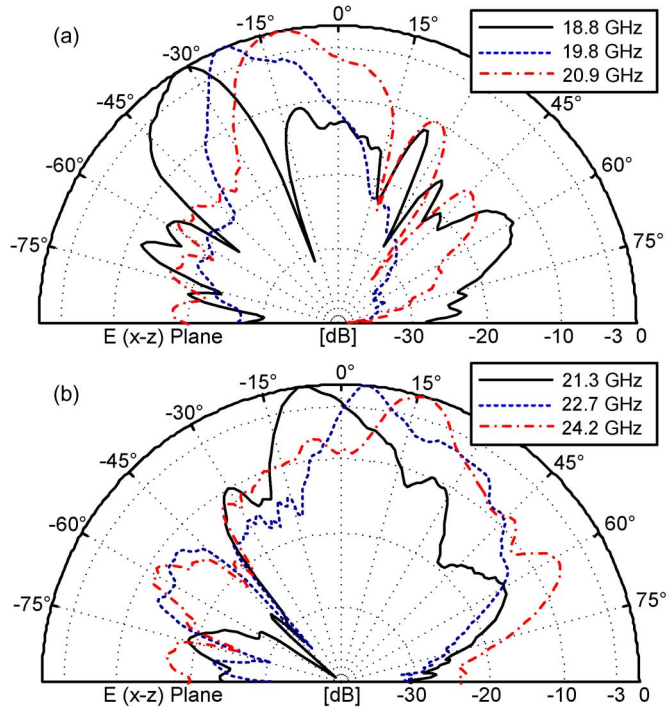

Fig. 18. Measured beam patterns from $-32°$ to $+17°$ for Design B. Patterns were normalized to the observed maximum at each frequency.

with no transition. In addition, Design B also offers an improved antenna match at 24.5 GHz when compared to Design A. Radiation efficiency [Realized antenna gain (which includes reflection losses)] values approach 50 and 90% [11.5 and 15.2 dBi] at this frequency as shown in Fig. 14 for Design A and Design B, respectively.

The simulated leakage rate for each cell in the transition section is shown in Fig. 15 with results also compared to that of the Nth unit cell. It can be observed that the leakage rate for the 1st cell [Nth cell] is below [above] 0.2 Nepers. Therefore the transition from the non-modulated printed line to the fifth unit cell within the structure allows for gradual power leakage along the antenna aperture.

Similar phase constant values were achieved for the unit cells within the transition section when compared to that of the Nth unit cell. This is an important point, mainly to ensure that all parts of the aperture radiate at the same beam angle as a function of frequency [5], [6]. In particular, minor variations were observed for the positions of the open LW stopbands and this is further outlined in Table I. For instance, for the 1^{st} unit cell [Nth unit cell] the LW stop band region was centered at 24.38 GHz [23.01 GHz] for the reduced [nominal] modulation factor M_u of 0.0677 [0.1867].

Further improvements in the operation of the LWAs can be achieved if the spatial periodicity along the u-direction is not maintained, as in this work, but varied. This additional design step for the transition section would ensure that the center frequency of the LW stop band, exhibited by each unit cell, was consistent and without variation. This further design iteration is possible since the position of the bandstop frequencies are both simultaneously controlled by ε_{eff} and D_u as discussed in Section III. Regardless of these suggested improvements, good radiation performance values are observed for the full-wave simulations of Design A and Design B. For example, simulated power gains of 15 dBi are realized as well as radiation efficiencies of almost 90% for Design B as shown in Figs. 14 and 16.

D. Antenna Measurements & Discussions

Measured realized gain and pointing angle values are plotted as a function of frequency in Fig. 16 for Design A and Design B. Very good performance values can be observed with continuous beam scanning through broadside from backfire to forward-fire; i.e. from 19 to 26 GHz with pointing angles ranging from $-20°$ to $+38°$. Cross-polarization levels are 10 dB below the main co-polarized maximum. Simulated and measured patterns are compared in Fig. 17 and side-lobe levels can be observed 16 dB below the main broadside beam. Additional beam pattern measurements are also shown in Fig. 18. Agreement can be observed with the measurements and simulations, in particular the pointing angle range for broadside radiating frequencies ($\theta_p \approx 0°$) which is centered at 23 GHz. This corresponds very well with the theoretical pointing angles calculated using the DD. However, when comparing the 50-Ω input match of the planar LWAs, a minor downward shift in frequency (of $\approx$1.5 GHz) can be observed as shown in Figs. 16 and 17. This effect is a likely result of fabrication tolerances, a higher than expected relative dielectric constant, and substrate anisotropy [43], [44]. These noted effects are further examined in Appendix III.

Both LWAs achieved gain values greater than 10 dBi at 20.5 GHz with Design B offering improved antenna gain from 21.9 to 22.3 GHz when compared to Design A. In addition, Design B also offers reduced reflection losses as shown in Fig. 19; i.e. $|S_{11}| < -20$ dB at 22.0 GHz for Design B while for Design A, $|S_{11}| > -10$ dB. Gain values are less [greater] than 10 dBi for Design A [B] in this range as shown in Fig. 16. However, it

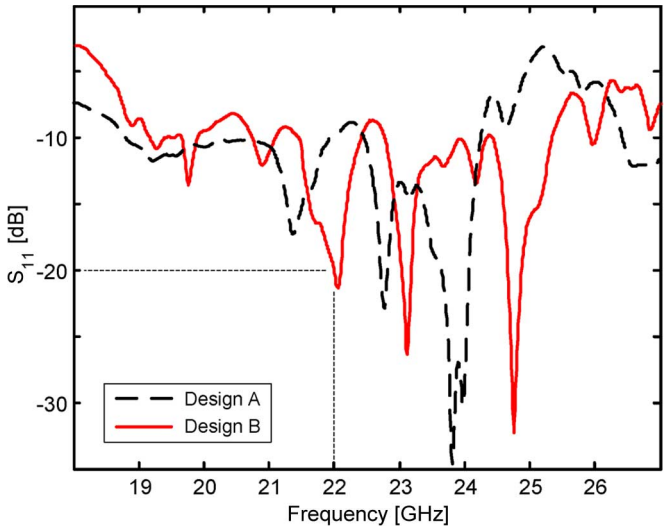

Fig. 19. Measured reflection coefficients. Better antenna matching can be observed for Design B when compared to Design A. For example, $|S_{11}| > -4$ dB at 25 GHz [$|S_{11}| > -10$ dB at 22.0 GHz] for Design A while for Design B, $|S_{11}| < -15$ dB [$|S_{11}| < -20$ dB at 22.0 GHz].

should be noted that the position of the pointing angle is affected by the auxiliary microstrip lines as shown in Fig. 16 for Design B. This suggests that additional design and layout improvements are possible, as well as more accurate synthesis procedures and theoretical modeling approaches that further take into consideration the radial construction. Regardless, the expected trend is observed in that Design B can offer increased gain and improved antenna matching when compared to Design A.

VI. Conclusion

Planar SW driven LWA structures, defined by a radial aperture of microstrip lines, are presented for frequency beam scanning and directive broadside radiation at microwave and millimeter wave frequencies. Two prototypes, Design A and Design B, are investigated with operation from 19 to 26 GHz and measured pointing angles ranging from $-20°$ to $+38°$ in the $\mathrm{E}(x-z)$ plane. Antenna performance is also improved by including a novel transition section near the origin for controlled LW radiation with radiation efficiencies that approach 50 and 90% for Designs A and B, respectively. To the authors' knowledge, this is the first time that such SW-fed LWAs have been investigated and experimentally verified, offering very good radiation performances, practical feeding, as well as ease of fabrication.

Since TM SWs are radially directed onto the guiding surface with coupling into the quasi-TEM mode of the host transverse microstrip guide, the phase constant can be engineered in such a way to exhibit particular dispersive behavior. This is achieved by the width variation, or modulation, of the printed microstrip lines defining a sinusoidally varying effective dielectric constant. Physically speaking, the incident TM SWs generated from the slot source are perturbed when directed onto the aperture. Leaky waves can be excited on this type of SMRS with pencil, and conical-sector beam patterns that scan as a function of frequency in the far-field.

The synthesis approach for the microstrip-based unit cell was outlined using the developed DD in terms of Mathieu's functions along with two main design goals: that the unit cell dimension should be made compact with respect to the operating wavelength and that the modulation factor should be small ($M_u \ll 1$). This ensures that the open LW stopband region is controlled with a reduced BW and that the sinusoidal variation of the effective dielectric constant is relatively small as to minimize reflections of the incident SWs. In addition, these design goals make certain that the presented theory is representative of the periodically modulated microstrip guide. Our design approach may also be applicable to other transmission line-based structures with sinusoidal variation of the effective material parameters as well as new printed circuits and quasi-uniform antennas for communication applications.

Appendix I
Current Distributions

Here we provide some further justifications for the 2-D grid assumption (Fig. 3) applied to the radial aperture for the LWA design investigated in this work (Design A and B as shown in Fig. 12) by investigating the generated current distributions due to the incident SWs excited by the SWL. For example, it would be expected that the dispersion characteristics of the single unit cell would be slightly altered from cell-to-cell with increasing distance from the origin and one would also assume that this effect could be fairly significant for Design A due to the absence of the auxiliary strips.

To illustrate this point compare two cells at a distance of $5D_u$ and $15D_u$ along the aperture as shown in Fig. 20(a) and (b). In particular, the cell at $5D_u$ is defined after the transition section with reference to Figs. 2 and 13. With such an increased distance from the origin for the 15th unit cell, in Design A, electromagnetic coupling between azimuthally adjacent cells (along the $\pm\phi$-directions) would likely decrease due to the increased arc length, and consequently, the radially directed waves generated at this point may experience an altered phase advance across the unit cell when compared to a position closer to the origin.

However, a very minor phase variation in current from cell-to-cell can be observed in Fig. 20 for both Design A and B. This suggests that a progressive and relatively uniform phase front is realized along the radial aperture. This is mainly due to the cylindrical waves generated by the SWL [9] as SWs are incident onto the periodic structure along the u-direction. This can also be observed in the current distribution shown in Fig. 20(c) near the origin (which corresponds to both Design A and Design B), meaning that a very minor field variation for the transverse magnetic field, H_t, can be realized along the aperture in the transverse ϕ-direction. Moreover, these observations imply that the theoretical developments and assumptions outlined in Sections II and III are a suitable engineering starting point for designing the unit cell, mainly because the considered LWAs (Design A and Design B) can be modeled and designed under a 2-D grid assumption when $M_u \ll 1$.

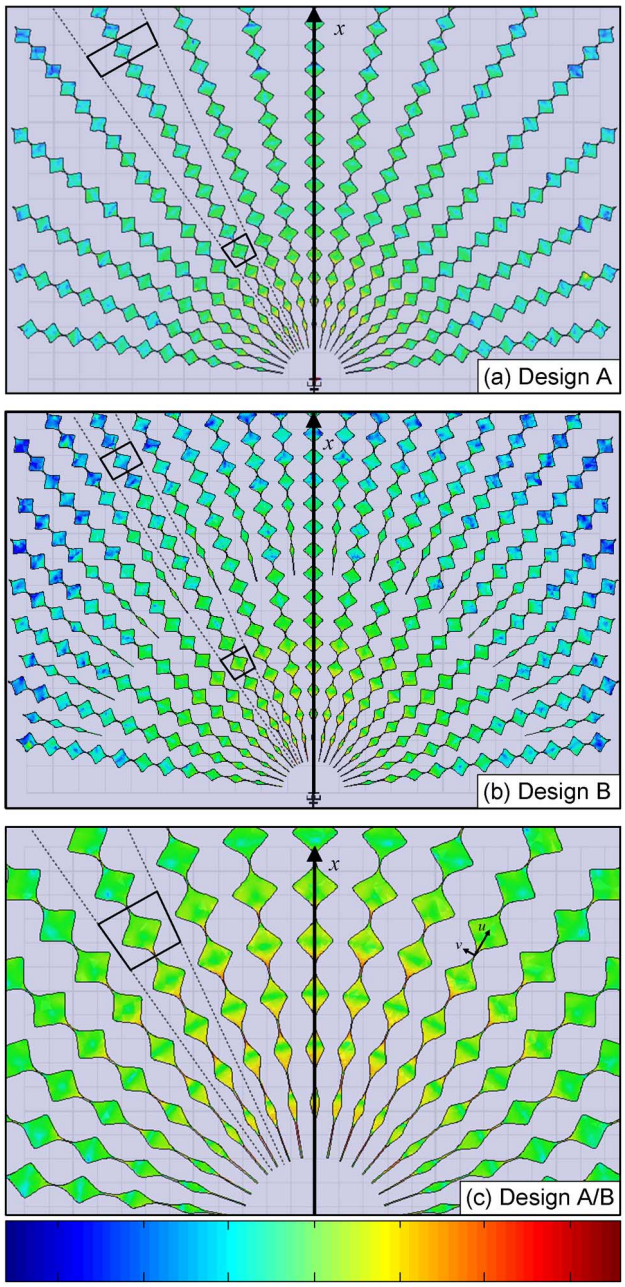

Fig. 20. Simulated current distributions (in A/m) generated on the longitudinal strips for Designs A and B at 24 GHz (for all plots red defines a maximum while blue defines a minimum). A uniform phase distribution can be observed as a function of radial distance from the origin with decreased amplitude. This suggests power leakage giving rise to directive beam patterns in the far-field.

Appendix II
Dispersive Properties of the Planar Guiding Structures

An explanation for the observed divergence between the theoretical and simulated pointing angle beyond 23 GHz in Fig. 10 could be related to the dispersive behavior of microstrip as frequency increases. For instance, the effective dielectric constant values collected during the parametric study used to synthesize the unit cell (Fig. 9), were based on a low frequency solution (approximately less than 10 GHz) and this was necessary to ensure accuracy of the results for the transverse-periodic guide,

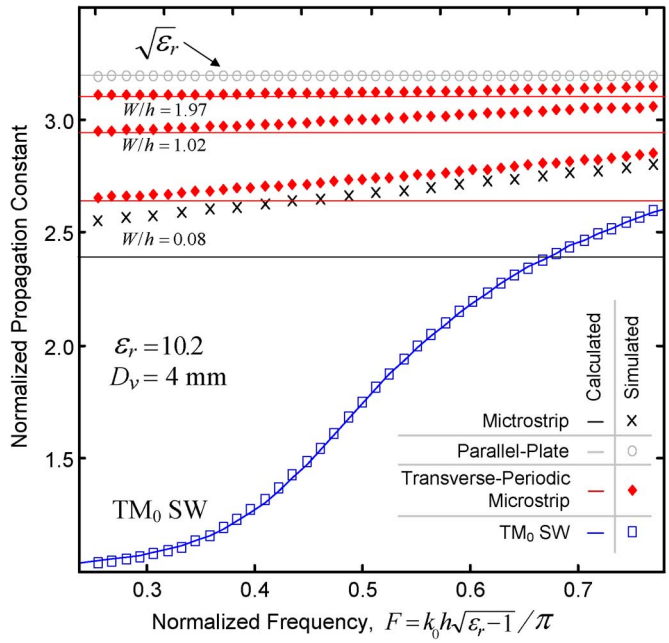

Fig. 21. Theoretical phase constants calculated for the fundamental microstrip mode[4] (with $W/h = 0.08$), the transverse periodic-microstrip guide (structure with no modulation), the TM_0 parallel-plate mode,[5] as well as the TM_0 SW mode of the slab. The horizontal lines (with $\hat{\beta} = \sqrt{\epsilon_e}$) for the transverse-periodic microstrip guide are calculated using the results obtained from the low frequency solution, i.e. Fig. 9. Results are also compared to full-wave HFSS simulations.

mainly, for comparison to the quasi-static solution of microstrip and the fundamental parallel-plate mode [29]. This simplification of the problem could explain the observed deviation in the pointing angle, and hence, the differences in β_u or θ_p for the calculations and simulations beyond 23 GHz.

To further investigate the dispersive behavior of the guides employed within the LWA designs, full-wave simulations of the normalized phase constants $\hat{\beta}(= \beta/k_0 = \sqrt{\epsilon_{eff}(\omega)})$ were completed and compared to numerical calculations. Results are plotted in Fig. 21. In particular, simulated $\hat{\beta}$ values for the transverse-periodic microstrip guide are shown and these simulations were completed considering an ideal TM SW source positioned at the origin (the simulation procedure is further described in Note 2). For completeness results are also compared to the quasi-TEM microstrip mode[4] (for $W/h = 0.08$) and both TM_0 fundamental modes of the parallel-plate guide[5] and the grounded slab, i.e. the TM_0 SW mode.

Slight divergence from the low frequency solution can be observed in Fig. 21. This observation may also explain the disagreement between the simulated and theoretical pointing angles of Fig. 10 beyond 23 GHz ($F > 0.6$). This dispersion effect is further examined in Fig. 22 where deviations from the low frequency solution approach 4% (for $W/h = 0.71$) at the upper operational frequency band limit of the LWA (about 26 GHz or $F = 0.67$). It should also be mentioned that, for the worst case, differences between the low frequency solutions approach 12% for the $W/h = 0.08$ transverse-periodic guide and when $F > 0.7$.

These minor discrepancies between the frequency dependent (simulated) phase constant and the low frequency approximations, which then cascaded into the design of the unit cell, are mainly a result of the dispersive properties of the host microstrip

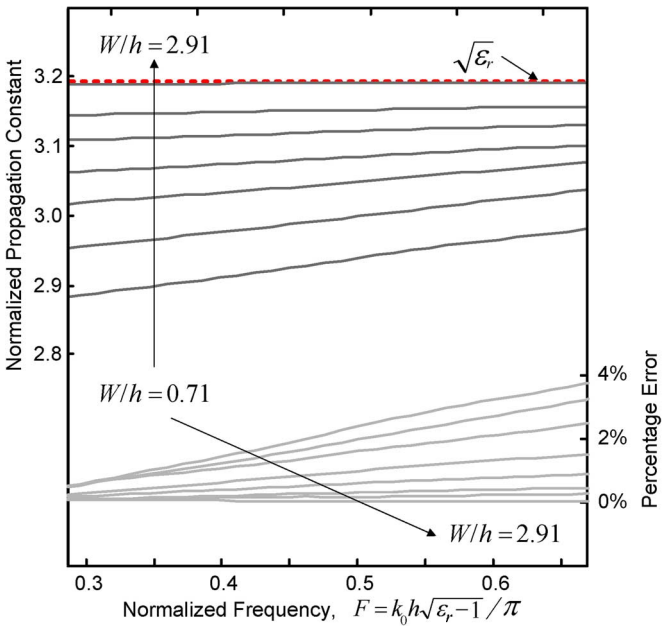

Fig. 22. Left axis: phase constant for the transverse periodic-microstrip guide (quasi-TEM mode with $D_v/h = 3.2$ and $\varepsilon_r = 10.2$) excited by TM SWs. The following strip widths: 0.9, 1.3, 1.7, 2.1, 2.5, 2.9, and 3.7 (all in mm) were investigated corresponding to a W/h range from 0.71 to 2.91. For comparison, the corresponding parallel-plate mode is also shown ($\hat{\beta} = \sqrt{\varepsilon_r}$, red dash line). Right axis: variation from the low frequency solution.

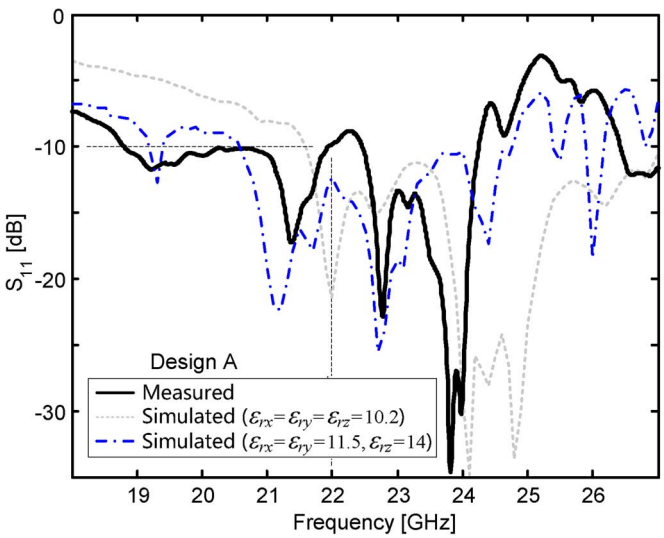

Fig. 23. Measured and simulated reflection coefficient for Design A. The downward frequency shift (≈1.5 GHz) can be observed in the minimums of $|S_{11}|$, for example, the simulated minimum at 24.8 [24.1] ⟨22.0⟩ GHz with the isotropic substrate model is observed in the measurements at 23.8 [22.8] ⟨21.3⟩ GHz. This downward shift is related to a higher dielectric constant value and substrate anisotropy [43].

guide. However, these minor discrepancies may be acceptable for antenna synthesis, since approximately 90% [35%] of the unit cell has a line width greater than 0.9 mm (or $W/h > 0.71$) [3.0 mm (or $W/h > 2.36$)]. This corresponds to errors in the calculated propagation constant for the transverse-periodic microstrip guide which are less than 4% [0.5%] and within the operational frequency range of the considered LWAs.

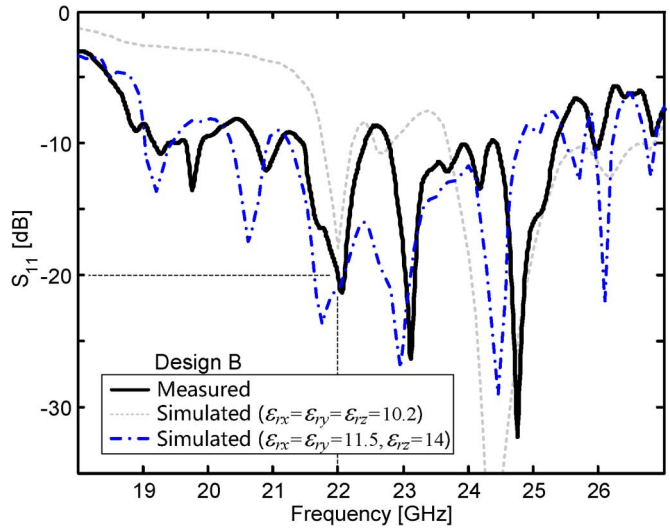

Fig. 24. Measured and simulated reflection coefficient for Design B.

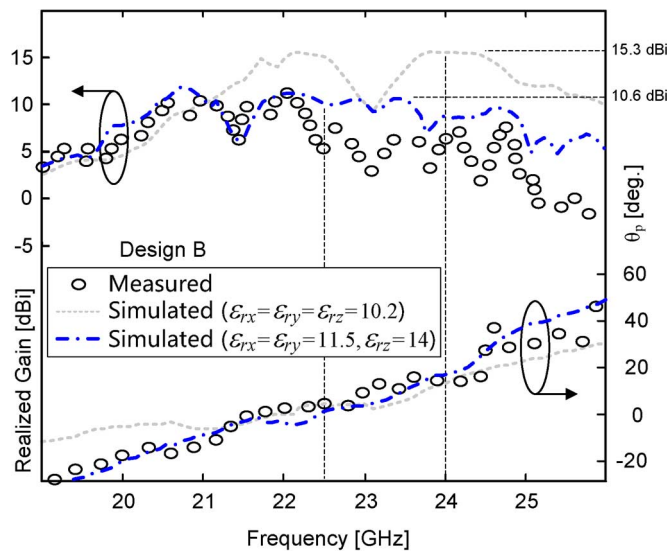

Fig. 25. Maximum gain and the pointing angle in the E plane for Design B.

Appendix III
Substrate Anisotropy

Better agreement between the measurements and simulations can be achieved if a tensor-based permittivity model with a higher dielectric constant is used in the full-wave simulations: $\varepsilon_{rx} = \varepsilon_{ry} = 11.5$ and $\varepsilon_{rz} = 14$, which is in contrast to the nominal value of $\varepsilon_r = 10.2$ for 6010.2LM as stated by Rogers Corporation [43]. For example, as shown in Fig. 23 the simulated minimum at 24.1 GHz ($|S_{11}| \leq -35$ dB) using the isotropic model ($\varepsilon_r = 10.2$) is reduced to 22.7 GHz ($|S_{11}| \leq -20$ dB) with the anisotropic model. This defines a downward frequency shift of approximately 1.5 GHz and this observed effect can be explained as substrate anisotropy for the electrically thick dielectric. Similar results can be also observed for Design B in Fig. 24. These observations can be further described as follows. For some substrates the relative dielectric constant in the vertical direction (ε_{rz}) can be different than that in the horizontal direction (ε_{rx} and ε_{ry}) and thus a tensor can be used to model the material [43]–[47]. This uniaxial anisotropy, which can be

significant for electrically thick substrates, is a result of manufacturing, and as indicated by [43] and documented in [44], can also have a frequency dependence. Further details on this phenomena are described in [45]–[47] and similar downward shifts in frequency have been reported by the authors for other LWA structures in [25] and [48].

Following this approach, the revised anisotropic simulation model gives better agreement with the far-field antenna measurements. For example, when gain and pointing angles are compared, as in Fig. 25, maximum gain values are 10.6 dBi at 22.5 GHz [15.3 dBi at 24 GHz] for Design B with $\varepsilon_{rx} = \varepsilon_{ry} = 11.5$ and $\varepsilon_{rz} = 14[\varepsilon_r = 10.2]$. This anisotropic effect appears to have caused a non-optimal modulation scheme (de-tuning) for the width modulated microstrip lines, moreover that, this type of LWA is sensitive to variations from the ideal (isotropic) substrate parameters as well as other fabrication tolerances. These results further suggest that dielectric anisotropy as well as the dispersive effects of guide should be taken into consideration to improve unit cell synthesis and antenna design for electrically thick substrates. These practicalities can explain the reduced gain values in the measurements as shown in Figs. 16 and 25 when compared to the full-wave simulations.

REFERENCES

[1] E. N. Leith, "Quasi-holographic techniques in the microwave region," in *Proc. IEEE*, Sep. 1971, vol. 59, no. 9, pp. 1305–1318.

[2] M. ElSherbiny, A. E. Fathy, A. Rosen, G. Ayers, and S. M. Perlow, "Holographic antenna concept, analysis, and parameters," *IEEE Trans. Antennas Propag.*, vol. 52, no. 3, pp. 830–839, Mar. 2004.

[3] D. Sievenpiper, J. Colburn, B. Fong, J. Ottush, and J. Visher, "Holographic artificial impedance surfaces for conformal antennas," in *Proc. IEEE Antennas Propag. Soc. Int. Symp. (APS-URSI)*, 2005, vol. 1B, pp. 256–259.

[4] A. Sutinjo, M. Okoniewski, and R. H. Johnston, "A holographic antenna approach for surface wave control in microstrip antenna applications," *IEEE Trans. Antennas Propag.*, vol. 58, no. 3, pp. 675–682, Mar. 2010.

[5] L. Matekovits, "Analytically expressed dispersion diagram of unit cells for a novel type of holographic surface," *IEEE Antennas Wireless Propag. Lett.*, vol. 9, pp. 1251–1254, 2010.

[6] C. A. Balanis, *Modern Antenna Handbook*. Hoboken, NY, USA: Wiley, 2011.

[7] M. Nannetti, F. Caminita, and S. Maci, "Leaky-wave based interpretation of the radiation from holographic surfaces," in *Proc. IEEE Antennas Propag. Society Intern. Symp. (APS-URSI)*, Honolulu, HI, USA, Jun. 2007, pp. 5813–5816.

[8] M. Ettorre, S. Bruni, G. Gerini, A. Neto, N. Llombart, and S. Maci, "Sector PCS-EBG antenna for low-cost high-directivity applications," *IEEE Antennas Wireless Propag. Lett.*, vol. 6, pp. 537–539, 2007.

[9] S. K. Podilchak, A. P. Freundorfer, and Y. M. M. Antar, "Planar leaky-wave antenna designs offering conical-sector beam scanning and broadside radiation using surface-wave launchers," *IEEE Antennas Wireless Propag. Lett.*, vol. 7, pp. 155–158, 2008.

[10] A. Ip and D. R. Jackson, "Radiation from cylindrical leaky waves," *IEEE Trans. Antennas Propag.*, vol. 38, no. 4, pp. 482–488, Apr. 1990.

[11] T. Zhao, D. R. Jackson, J. T. Williams, H. Y. D. Yang, and A. A. Oliner, "2D periodic leaky wave antennas—Part I: Metal patch design," *IEEE Trans. Antennas Propag.*, vol. AP-53, pp. 3505–3514, Nov. 2005.

[12] P. Burghignoli, G. Lovat, and D. R. Jackson, "Analysis and optimization of leaky-wave radiation at broadside from a class of 1-D periodic structures," *IEEE Trans. Antennas Propag.*, vol. 54, no. 9, pp. 2593–2604, Sep. 2006.

[13] S. K. Podilchak, L. Matekovits, A. P. Freundorfer, K. Esselle, and Y. M. M. Antar, "Modulated strip-line leaky-wave antenna using a printed grating lens and a surface-wave source," presented at the 14th Int. Symp. Antenna Technology and Applied Electromagnetics and the American Electromagnetics Conf., Jul. 5–8, 2010.

[14] A. M. Patel and A. Grbic, "A printed leaky-wave antenna based on a sinusoidally-modulated reactance surface," *IEEE Trans. Antennas Propag.*, vol. 59, no. 6, pp. 2087–2096, Jun. 2011.

[15] G. Minatti, F. Caminita, M. Casaletti, and S. Maci, "Spiral leaky-wave antennas based on modulated surface impedance," *IEEE Trans. Antennas Propag.*, vol. 59, no. 12, pp. 4436–4444, Dec. 2011.

[16] S. K. Podilchak, L. Matekovits, A. P. Freundorfer, Y. M. M. Antar, and M. Orefice, "A printed radial configuration of width-modulated striplines for controlled guided-wave radiation," in *Proc. 6th Eur. Conf. Antennas Propagation (EUCAP)*, Mar. 2012, pp. 2911–2913.

[17] T. Tamir, H. C. Wang, and A. A. Oliner, "Wave propagation in sinusoidally stratified dielectric media," *IEEE Trans. Microw. Theory Tech.*, vol. 12, no. 5, pp. 323–335, May 1964.

[18] C. Yeh, K. F. Casey, and Z. A. Kaprielian, "Transverse magnetic wave propagation in sinusoidally stratified dielectric media," *IEEE Trans. Microw. Theory Tech.*, vol. 13, pp. 297–302, May 1965.

[19] A. Hessel, *General Characteristics of Traveling-Wave Antennas, in Antenna Theory, Part 2*, Collin and Zucker, Eds. New York, NY, USA: McGraw-Hill, 1969.

[20] P. R. Villeneuve and M. Piché, "Photonic band gaps of transverse-electric modes in two-dimensionally periodic media," *J. Opt. Soc. Amer. A*, vol. 8, no. 8, pp. 1296–1304, Aug. 1991.

[21] C. C. Rodney, "Demonstration of wave propagation in a periodic structure," *Amer. J. Phys.*, vol. 53, no. 6, pp. 563–567, Jun. 1985.

[22] L. Matekovits, G. V. Colomé, and M. Orefice, "Controlling the bandlimits of TE-surface wave propagation along a modulated microstrip-line-based high impedance surface," *IEEE Trans. Antennas Propag.*, vol. 56, no. 8, pt. 2, pp. 2555–2562, Aug. 2008.

[23] L. Matekovits, I. Peter, S. K. Podilchak, A. P. Freundorfer, K. Esselle, and Y. M. M. Antar, "Effects of the variation of the dielectric constant for a periodic, width-modulated microstrip line based sensor," presented at the IEEE Antennas and Propag. Society Intern. Symp., Jul. 11–17, 2010.

[24] S. Mahmoud, Y. M. M. Antar, H. Hammad, and A. P. Freundorfer, "Theoretical considerations in the optimization of surface waves on a planar structure," *IEEE Trans. Antennas Propag.*, vol. 52, no. 8, pp. 2057–2063, Apr. 2004.

[25] S. K. Podilchak, A. P. Freundorfer, and Y. M. M. Antar, "Surface-wave launchers for beam steering and application to planar leaky-wave antennas," *IEEE Trans. Antennas Propag.*, vol. 57, pp. 355–363, Feb. 2009.

[26] G. Floquet, "Sur les équations différentielles linéaires à coefficients périodiques," *Annales de l'École Normale Supérieure*, vol. 12, pp. 47–88, 1883.

[27] L. Brillouin, *Wave Propagation in Periodic Structures*. New York, NY, USA: Dover, 1953.

[28] *"High Frequency Structure Simulator"* ver. 13.0, Ansoft Corp, 2013 [Online]. Available: www.ansys.com

[29] D. M. Pozar, *Microwave Engineering, Fourth Edition*. Hoboken, NJ, USA: Wiley, 2012.

[30] T. Itoh and R. Mittra, "Spectral-domain approach for calculating the dispersion characteristics of microstrip lines," *IEEE Trans. Microw. Theory Tech.*, vol. 21, pp. 496–499, Jul. 1973.

[31] I. J. Bahl and D. K. Trivedi, "A designer's guide to microstrip line," *Microwaves*, pp. 174–182, May 1977.

[32] K. C. Gupta, R. Garg, and I. J. Bahl, *Microstrip Lines and Slotlines*. Dedham, MA, USA: Artech House, 1979.

[33] E. Mathieu, "Memoire sur le mouvement vibratorie dune membrane de forme elliptique," *J. d. Math Pures et Appliquees*, ser. 2, vol. 13, pp. 137–203, 1868.

[34] T. Tamir, "Characteristic exponents of Mathieu functions," *Math. Comput.*, vol. 16, pp. 100–106, Jan. 1962.

[35] N. W. McLachlan, *Theory and application of Mathieu Functions*. New York, NY, USA: Dover Publications, 1964.

[36] M. Abramowitz and A. Stegun, *Handbook of Mathematical Functions with Formulas, Graphs, and Mathematical Tables*. Mineola, NY, USA: Dover Publications, 1972.

[37] J. C. Gutiérrez-Vega, R. M. Rodríguez-Dagnino, M. A. Meneses-Nava, and S. Chávez-Cerda, "Mathieu functions, a visual approach," *Amer. J. Phys.*, vol. 71, no. 3, pp. 233–242, Mar. 2003.

[38] J. S. Gomez-Diaz, D. Canete-Rebenaque, and A. Álvarez-Melcón, "A simple CRLH LWA Circuit condition for constant radiation rate," *IEEE Antennas Wireless Propag. Lett.*, vol. 10, pp. 29–32, 2011.

[39] S. Otto, A. Rennings, K. Solback, and C. Caloz, "Transmission line modeling and asymptotic formulas for periodic leaky-wave antennas scanning through broadside," *IEEE Trans. Antennas Propag.*, vol. 59, no. 10, pp. 3695–3709, Oct. 2011.

[40] S. Otto, A. Al-Bassam, A. Rennings, K. Solbach, and C. Caloz, "Radiation efficiency of longitudinally symmetric and asymmetric periodic leaky-wave antennas," *IEEE Antennas Wireless Propag. Lett.*, vol. 11, pp. 612–615, 2012.

[41] *CST Microwave Studio* ver. 2012, CST Computer Simulation Technology AG,, 2012 [Online]. Available: www.cst.com
[42] L. Matekovits, G. V. Colomé, and M. Orefice, "Effect of transverse periodicity on the value of the effective dielectric constant for a microstrip line," in *Proc. IEEE Antennas Propag. Society Int. Symp. (APSURSI)*, Jun. 9–15, 2007, pp. 189–192.
[43] Personal Communication with Dr. Allen F. Horn, Lurie R&D Center Jun. 2013.
[44] R. Garg, P. Bhartia, I. Bahl, and A. Ittipiboon*, Microstrip Antenna Design Handbook*. Norwood, MA, USA: Artech House, 2001.
[45] N. G. Alexopoulos, "Integrated-circuit structures on anisotropic substrates," *IEEE Trans. Microwave Theory Tech.*, vol. 35, no. 10, pp. 847–881, Oct. 1985.
[46] D. Pozar, "Radiation and scattering from a microstrip patch on a uniaxial substrate," *IEEE Trans. Antennas Propag.*, vol. 35, pp. 613–621, Jun. 1987.
[47] J. C. Rautio, R. L. Carlson, B. J. Rautio, and S. Arvas, "Shielded dual-mode microstrip resonator measurement of uniaxial anisotropy," *IEEE Trans. Microwave Theory Tech.*, vol. 59, no. 3, pp. 748–754, Mar. 2011.
[48] S. K. Podilchak, P. Baccarelli, P. Burghignoli, A. P. Freundorfer, and Y. M. M. Antar, "Optimization of a planar 'bull-eye' leaky-wave antenna fed by a printed surface-wave source," *IEEE Antennas Wireless Propag. Lett.*, vol. 12, pp. 665–669, 2013.

Symon K. Podilchak (S'03–M'05) received the B.A.Sc. degree in engineering science from the University of Toronto, ON, Canada, in 2005 and the M.A.Sc., and Ph.D. degree in electrical engineering from The Royal Military College of Canada (RMC), Kingston, ON, and Queen's University (QU), Kingston, ON, in 2008 and 2013, respectively.

Since 2010 he has been a Teaching Fellow at QU where he has contributed to the development and teaching of electromagnetics and electronics based courses at the graduate and undergraduate level. Currently he is an Adjunct Lecturer at QU in the Department of Electrical and Computer Engineering. During this same period he has also been a Research Associate at RMC. Dr. Podilchak has also had experience as a computer programmer, technology investment analyst, and assisted in the design of radomes for 77 GHz automotive radar. Recent industry experience also includes modeling the radar cross-section of military vessels for high frequency surface-wave radar, professional software design and implementation for measurements in anechoic chambers, and the research and development of highly compact circularly polarized antennas for microsatellites. His research interests include the analysis and design of planar surface-wave and leaky-wave structures, UWB antennas, metamaterials, millimeter-wave CMOS integrated circuits, and measurement techniques for antennas.

Dr. Podilchak is a registered Professional Engineer (P.Eng.) in the Province of Ontario. He has been the recipient of many best paper awards and scholarships; most notably Graduate Research Fellowships from the IEEE Antennas and Propagation Society and the IEEE Microwave Theory and Techniques Society as well as three Young Scientist Awards from the International Union of Radio Science (URSI). In 2011 and 2013 he received student paper awards at the IEEE International Symposium on Antennas and Propagation, and in 2012, the best paper prize for antenna design at the European Conference on Antennas and Propagation.

Ladislau Matekovits (M'94–SM'11) was born in Arad, Romania, on November 19, 1967. He received the degree in electronic engineering from Institutul Politehnic din Bucureşti, Bucureşti, Romania, and the Ph.D. (Dottorato di Ricerca) in electronic engineering from Politecnico di Torino, Turin, Italy in 1992 and 1995, respectively.

Since 1995, he has been with the Electronics Department of the Politecnico di Torino, first with a postdoctoral fellowship, then as a Research Assistant. He joined the same Department as Assistant Professor in 2002 and was appointed as Senior Assistant Professor in 2005. In late 2005, he was a Visiting Scientist at the Antennas and Scattering Department of the FGAN-FHR (now Fraunhofer Institute), Wachtberg, Germany. From 2009 to 2012, he was a Marie Curie Fellow two of those years spent at Macquarie University, Sydney, NSW, Australia, where now he holds a visiting academic position. He teaches electromagnetic field theory and conducts research in the development of computational techniques for numerical analysis of printed antennas and electromagnetic scattering. He is (co-)author of more than 200 publications in the area of theoretical and experimental studies of new, numerically efficient and fast full-wave techniques to analyze large arrays, optimization techniques, active and passive metamaterials and dispersion engineering. He has delivered seminars on these topics all around the world: Europe, USA (AFRL/MIT-Boston), Australia.

Dr. Matekovits is a recipient of various awards in international conferences, including the 1998 URSI Young Scientist Award (Thessaloniki, Greece), the Barzilai Award 1998 (Young Scientist Award, granted every two years by the Italian National Electromagnetic Group), and the Best AP2000 Oral Paper on Antennas, ESA-EUREL Millennium Conference on Antennas & Propagation (Davos, Switzerland). He is member of several conferences program committees. He was Assistant Chairman and Publication Chairman of the European Microwave Week 2002 (Milan, Italy). He serves as a reviewer for different journals, including the IEEE TRANSACTIONS ON ANTENNAS AND PROPAGATION and the *IEEE Antennas and Wireless Propagation Letters*.

Alois P. Freundorfer (SM'90) received the B.A.Sc., M.A.Sc., and Ph.D. degrees from the University of Toronto, Toronto, ON, Canada, in 1981, 1983, and 1989, respectively.

In 1990, he joined the Department of Electrical Engineering, Queens University, Kingston, ON, Canada. Since then he has done work in nonlinear optics of organic crystals, coherent optical network analysis as well as microwave integrated circuits. Currently he is focusing his attention on monolithic microwave circuits used in lightwave systems with bit rates in excess of 20 Gb/s and on monolithic millimeter wave integrated circuits used in wireless communications.

Yahia M. M. Antar (S'73–M'76–SM'85–F'00) received the B.Sc. (hons.) degree from Alexandria University, Alexandria, Egypt, in 1966 and the M.Sc. and Ph.D. degrees from the University of Manitoba, Winnipeg, Canada, in 1971 and 1975, respectively, all in electrical engineering.

In 1977, he was awarded a Government of Canada Visiting Fellowship at the Communications Research Centre in Ottawa where he worked with the Space Technology Directorate on communications antennas for satellite systems. In May 1979, he joined the Division of Electrical Engineering, National Research Council of Canada, Ottawa, where he worked on polarization radar applications in remote sensing of precipitation, radio wave propagation, electromagnetic scattering and radar cross section investigations. In November 1987, he joined the staff of the Department of Electrical and Computer Engineering at the Royal Military College of Canada in Kingston, where he has held the position of Professor since 1990. He has authored or co-authored close to 200 journal papers, many chapters in books, about 400 refereed conference papers, holds several patents, chaired several national and international conferences and given plenary talks at many conferences. He has supervised and co-supervised over 80 Ph.D. and M.Sc. theses at the Royal Military College and at Queen's University, of which several have received the Governor General of Canada Gold Medal, the outstanding Ph.D. thesis of the Division of Applied Science as well as many best paper awards in major international symposia. He held an adjunct appointment at the University of Manitoba and has a cross appointment at Queen's University in Kingston. He also serves, since November 2008, as Associate Director of the Defence and Security Research Institute (DSRI).

Dr. Antar is a Fellow of the IEEE, the Engineering Institute of Canada (FEIC), and the Electromagnetic Academy. He served as the Chairman of the Canadian National Commission for Radio Science (CNC, URSI, 1999–2008), Commission B National Chair (1993–1999). In May 2002, he was awarded a Tier 1 Canada Research Chair in Electromagnetic Engineering which has been renewed in 2009. In 2003 he was awarded the Royal Military College of Canada "Excellence in Research" Prize and in 2012 the Class of 1965 Teaching Excellence award. He was elected by the Council of the International Union of

Radio Science (URSI) to the Board as Vice President in August 2008, and to the IEEE Antennas and Propagation Society Administration Committee in December 2009. On 31 January 2011, he was appointed Member of the Canadian Defence Science Advisory Board (DSAB). He is an IEEE Antennas and Propagation Society Distinguished Lecturer. In October 2012 he received from the Governor General of Canada the Queen's Diamond Jubilee Medal in recognition for his contribution to Canada. He serves as an Associate Editor (Features) of the *IEEE Antennas and Propagation Magazine*, served as Associate Editor of the IEEE TRANSACTIONS ON ANTENNAS AND PROPAGATION, *IEEE Antennas and Wireless Propagation Letters*, and was a member of the Editorial Board of the RFMiCAE Journal. He served on NSERC grants selection and strategic grants committees, Ontario Early Research Awards (ERA) panels, and on review panels for the National Science Foundation.

Mario Orefice (M'82–SM'10) is a Professor of electromagnetic waves and antennas, and Founder and Director of the Laboratory of Antennas and EMC (LACE), Department of Electronics and Telecommunications, Politecnico di Torino, Italy.

He is the author or coauthor of more than 200 publications in the area of theoretical and experimental studies on antennas and applied electromagnetics, in particular on waveguide discontinuities, reflector antennas, waveguide arrays and printed antennas, often in the frame of international projects, Networks of Excellence and university-industry partnerships. His most recent research activities are on automotive and miniaturized antennas, with particular interest on the bandwidth performance, and on reflector antennas and reflectarrays for millimeter waves.

Prof. Orefice is also strongly committed to many international scientific activities: he was on the Steering Committee and a Reviewer of several international journals and conferences; founder in 1989 and Chairman up to 1998 of the ICEAA (International Conference on Electromagnetics in Advanced Applications); General Chairman of the European Microwave Week in 2002 and of EuCAP (European Conference on Antennas and Propagation) in 2011.